Univerzita Karlova v Praze
Matematicko-fyzikální fakulta

BAKALÁŘSKÁ PRÁCE

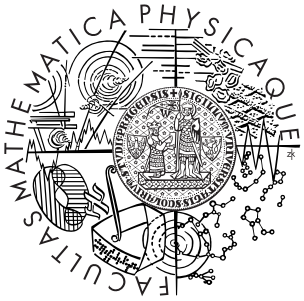

Pavel Motloch

Výpočet relativistické pásové struktury vrstvy Fe/Ga(Mn)As metodou těsné vazby a studium jejích magnetických vlastností

Ústav teoretické fyziky

Vedoucí bakalářské práce: Mgr. Tomáš Jungwirth, Dr.
Fyzikální ústav AV ČR, v.v.i.

Studijní program: Fyzika, Obecná fyzika

2010

Na tomto místě bych chtěl poděkovat všem, kteří mi pomáhali při psaní této práce:

Mgr. Tomáši Jungwirthovi, Dr., vedoucímu mé bakalářské práce, za odborné vedení a množství podnětných nápadů;

Mgr. Janu Zemenovi za každou z tisíce praktických rad;

Janu Maškovi, Csc. za zkušenosti s metodou těsné vazby, které mi předal;

a své rodině za neocenitelnou, neustálou a nevyčerpatelnou podporu.

Prohlašuji, že jsem svou bakalářskou práci napsal samostatně a výhradně s použitím citovaných pramenů. Souhlasím se zapůjčováním práce a jejím zveřejňováním.

V Praze dne 30. 7. 2010 Pavel Motloch

Table of Contents

Název práce: Výpočet relativistické pásové struktury vrstvy Fe/Ga(Mn)As metodou těsné vazby a studium jejích magnetických vlastností
Autor: Pavel Motloch
Katedra (ústav): Ústav teoretické fyziky
Vedoucí bakalářské práce: Mgr. Tomáš Jungwirth, Dr.; FZÚ AV ČR, v.v.i.
e-mail vedoucího: jungw@fzu.cz

Abstrakt: V předložené práci studujeme magnetokrystalické anizotropie tenkých vrstev Fa/GaAs a Fe/Ga(Mn)As metodou těsné vazby. Výzkum takovýchto hybridních kovovo-polovodičových rozhraní je motivován jejich značným technickým potenciálem pro využití spinového stupně volnosti v moderních elektronických součástkách. První část této práce je věnována nástinu metody těsné vazby v "two-center approximation". Dále popisujeme náš počítačový program, schopný provádět různé výpočty metodou těsné vazby pro dvou- a třírozměrné struktury a který tvoří součást této práce. V poslední části shrnujeme naše zkoumání magnetokrystalických anizotropií tenkých železných vrstev na GaAs a Ga(Mn)As.

Klíčová slova: metoda těsné vazby, magnetokrystalická anizotropie,
Fe/Ga(Mn)As, tenké vrstvy

Title: Relativistic tight-binding band-structure calculation of a multilayer Fe/Ga(Mn)As and study of its magnetic properties
Author: Pavel Motloch
Department: Institute of Theoretical Physics
Supervisor: Mgr. Tomáš Jungwirth, Dr.; FZÚ AV ČR, v.v.i.
Supervisor's e-mail address: jungw@fzu.cz

Abstract: In the present work we study magnetocrystalline anisotropies of thin iron films on GaAs and Ga(Mn)As substrates using the tight binding method. Investigation of these hybrid semiconductor-metal structures is motivated by their great technical potential for utilizing spin degree of freedom in modern electronic devices. The first part of this work is dedicated to an outline of the tight binding method in the two-center approximation. Further we describe our computer program that is capable to perform various tight-binding calculations for both two- and three-dimensional structures and which was written as a part of the work. In last chapters we report on our investigations of magnetocrystalline anisotropies of thin iron films on GaAs and Ga(Mn)As.

Keywords: tight binding method, magnetocrystalline anisotropy,
Fe/Ga(Mn)As, thin films

Chapter 1

The Tight Binding Method

1.1 Preliminaries

To understand a crystalline material fully, one should in principle solve the Dirac equation for the system of all electrons and nuclei in the material. Due to the clear impossibility of this task, it is necessary to use numerous simplifications.

Because the masses of the atoms are far greater than the mass of the electron, we neglect the kinetic energy of the atoms and consider them as fixed in positions $\mathbf{R}_j$, making up an ideal crystal lattice. [1] This approximation corresponds to taking zero absolute temperature and neglecting the ratio of the electronic mass to the masses of the nuclei involved.

Local density approximation (LDA) theory recasts the complicated many-electron problem into an effective non-interacting model of electrons in the field produced by the lattice ions and in the self-consistent Kohn-Sham LDA fields corresponding to the direct Coulomb, exchange, and correlation energies of the many-electron system. Both the ion and Kohn-Sham effective one-particle potentials have the periodicity of the underlying crystal. Therefore, we can focus our attention to the single particle problem of an electron governed by the Hamiltonian

$$H(\mathbf{r}) = -\frac{\hbar^2}{2M_e}\Delta + \sum_j V(\mathbf{r} - \mathbf{R}_j)\,, \tag{1.1}$$

where the first term describes the kinetic energy of the electron of mass M_e and the second term is the effective one-particle potential with the periodicity of the lattice. We have written this effective potential in a form of a sum of terms assumed to originate from individual atoms in the lattice at positions $\mathbf{R}_j$. This form of the

[1] We assume, without loss of generality that one of the atoms is placed in the origin of Cartesian coordinates.

Hamiltonian is the basis of the tight-binding method of band structure calculations used in the thesis. [2]

1.2 Tight binding method

The principles of the tight binding method[3] can be most clearly explained on the example of a material with a single atom in its unit cell. Let's for the moment consider this case.

In the tight binding method, we assume that the set of orthogonal solutions of the atomic problem

$$\left(-\frac{\hbar^2}{2M_e}\Delta + V\right)\psi_n(\mathbf{r}) = \varepsilon_n\psi_n(\mathbf{r}) \tag{1.2}$$

is known for the atoms forming the crystalline material. Solutions to the single electron problem defined by the Hamiltonian (1.1) are then searched for in form of the linear combination of the Bloch sums

$$\Psi_{\mathbf{k}}(\mathbf{r}) = \sum_{j,n} v_n \exp[i\mathbf{k}\cdot\mathbf{R}_j]\psi_n(\mathbf{r}-\mathbf{R}_j)\,, \tag{1.3}$$

with vector $\mathbf{k}$ being in the first Brillouin zone (BZ).

If we substitute this ansatz into the Schrödinger equation

$$H\Psi_{\mathbf{k}}(\mathbf{r}) = \varepsilon(\mathbf{k})\Psi_{\mathbf{k}}(\mathbf{r})\,, \tag{1.4}$$

multiply both sides of the equation with $\psi_m^*(\mathbf{r})$ and integrate over space, then we get an infinite set of linear equations for an infinite number of unknown coefficients v_n:

$$\begin{aligned}\sum_{n,j} v_n \exp[i\mathbf{k}\cdot\mathbf{R}_j]\int d^3r\psi_m^*(\mathbf{r})H\psi_n(\mathbf{r}-\mathbf{R}_j) = \\ = \varepsilon(\mathbf{k})\sum_{n,j} v_n \exp[i\mathbf{k}\cdot\mathbf{R}_j]\int d^3r\psi_m^*(\mathbf{r})\psi_n(\mathbf{r}-\mathbf{R}_j)\,.\end{aligned} \tag{1.5}$$

[2] In cases, when we consider more atoms in a unit cell, we must add sum over all atoms in the unit cell.

[3] The general description of the tight binding method can be found for example in sources [1, 2, 3]. Unless explicitly stated, all information provided in this section and the directly following one comes from these sources.

After introducing matrices with elements

$$H_{m,n}(\mathbf{k}) = \sum_j \exp[i\mathbf{k}\cdot\mathbf{R}_j] \int d^3r \psi_m^*(\mathbf{r}) H \psi_n(\mathbf{r}-\mathbf{R}_j) \tag{1.6}$$

$$S_{m,n}(\mathbf{k}) = \sum_j \exp[i\mathbf{k}\cdot\mathbf{R}_j] \int d^3r \psi_m^*(\mathbf{r}) \psi_n(\mathbf{r}-\mathbf{R}_j)\,, \tag{1.7}$$

we can rewrite equation (1.5) in the matrix form

$$H(\mathbf{k})v = E(\mathbf{k})S(\mathbf{k})v\,, \tag{1.8}$$

with v being the column vector of coefficients c_n,

$$v = \begin{pmatrix} c_1 \\ c_2 \\ c_3 \\ \vdots \end{pmatrix}. \tag{1.9}$$

Löwdin [4] found out that we can save laborious efforts by replacing original ψ_n with wavefunctions

$$\phi_n(\mathbf{r}) = \sum_{m,j} O^{-1/2}_{nm,j} \psi_m(\mathbf{r}-\mathbf{R}_j)\,, \tag{1.10}$$

where the matrix O has elements

$$O_{nm,j} = \exp[i\mathbf{k}\cdot\mathbf{R}_j] \int d^3r \psi_m^*(\mathbf{r}) \psi_n(\mathbf{r}-\mathbf{R}_j)\,. \tag{1.11}$$

When we interchange original atomic wavefunctions ψ_n for Löwdin functions ϕ_n in the ansatz (1.3), then the corresponding overlap matrix S with elements

$$S_{m,n}(\mathbf{k}) = \sum_j \exp[i\mathbf{k}\cdot\mathbf{R}_j] \int d^3r \phi_m^*(\mathbf{r}) \phi_n(\mathbf{r}-\mathbf{R}_j) \tag{1.12}$$

will be equal to δ_{mn}. This way we arrive at the equation

$$H(\mathbf{k})v = \varepsilon(\mathbf{k})v\,, \tag{1.13}$$

which is just a common secular equation. Under $H(\mathbf{k})$ in (1.13) we naturally understand expression in Eq. (1.6) with ψ replaced by ϕ,

$$H_{m,n}(\mathbf{k}) = \sum_j \exp[i\mathbf{k}\cdot\mathbf{R}_j] \int d^3r \phi_m^*(\mathbf{r}) H \phi_n(\mathbf{r}-\mathbf{R}_j)\,. \tag{1.14}$$

As was shown by Slater and Koster [5], these newly formed Löwdin functions ϕ show the same symmetry properties as the original atomic orbitals do. The problem connected with the transition from atomic orbitals to Löwdin functions is that we lose the localization of the wavefunctions. Orbitals $\psi_n(\mathbf{r} - \mathbf{R}_j)$ can be perceived as being "localized" in the vicinity of site $\mathbf{R}_j$. After performing the transformation (1.10), the resulting functions ϕ will be "extended" over a larger amount of space, making physical interpretation of results more difficult. However, in cases where overlap integrals (1.7) are small in comparison to unity, we can neglect the difference between the S- matrix and the unit matrix and make another approximation in considering

$$\phi = \psi \,. \tag{1.15}$$

In this case, the basic wavefuncitons will still be very well localized.

To make calculations possible, we consider only a finite number of atomic orbitals involved in the sum (1.3), instead of an infinite number. The choice of orbitals involved is made for each material separetely, depending on which properties we are interested in and which orbitals are physically relevant for the problem. Typically we consider orbitals with energies in the vicinity of the Fermi energy of the material, usually the orbitals in the partially filled electron shells. After this simplification, matrix H of the equation (1.13) has only finite dimensions.

This simplification is motivated by the two facts: The orbitals with energies high above the Fermi energy remain unfilled, because the electrons do not have energies necessary for excitations to these levels. On the other hand, electrons in closed shells are rather tightly bound to the nucleus and do not respond to the presence of other atoms greatly. Therefore, we can neglect existence of both these types of orbitals, focusing our attention to the orbitals of the partially filled shells and filled and empty shells near the Fermi energy.

1.3 More atoms in the unit cell

So far we were considering systems with a single atom in their unit cell, now we turn our attention to the cases in which we are considering systems with r atoms in a unit cell. We take the unit cell that includes origin and label relative positions of the r atoms within it by vectors $\mathbf{R}_\alpha$.[4] Position of each atom in the material can then be uniquely decomposed into a sum of a single vector $\mathbf{R}_\alpha$ and a single vector $\mathbf{R}_j$.

In solving the problem, we proceed in direct analogy — instead of eq. (1.3) we

[4]Greek indices will always denote positions of atoms with respect to their accompanying unit cell, Roman indices denote vectors of the underlying Bravais lattice.

search for the solutions in the form

$$\Psi_{\mathbf{k}}(\mathbf{r}) = \sum_{j,n,\alpha} v_{n,\alpha} \exp[i\mathbf{k}\cdot(\mathbf{R}_j + \mathbf{R}_\alpha)]\phi_{n,\alpha}(\mathbf{r} - \mathbf{R}_\alpha - \mathbf{R}_j)\,, \tag{1.16}$$

where we add summing over all atoms α in the unit cell. Here we denoted $\phi_{n,\alpha}$ n-th atomic wave function of the atom positioned at $\mathbf{R}_\alpha$.

After this ansatz, we again arrive at the equation (1.13), but this time the elements of the Hamiltonian matrix and vector v are numbered with an ordered pair (n, α). We have many possibilities by which we can assign these pairs to the rows of the Hamiltonian and vector v. However, it is convenient to arrange all (n, α) in the way in which all pairs corresponding to the same position within the unit cell α are grouped together. In such case, the Hamiltonian matrix $H(\mathbf{k})$ naturally fragments into smaller blocks, each of which describes interactions between atoms positioned at different places in the unit cell.

The situation is visualized in Figure 1 on an example of bulk GaAs, in which case we have two atoms in the unit cell — one Ga atom and one As atom. After adopting the arrangement mentioned above, beginning the "numbering" of the matrix rows with the gallium orbitals (α = Ga) and then adding the orbitals of the arsenic, the Hamiltonian is clearly divided into four segments. One of them describes interactions between gallium atoms (Ga-Ga), one describes interactions between arsenic atoms (As-As) and the two remaining segments describe interactions between the gallium and arsenic atoms. The dimensions of each block are determined by the numbers of orbitals considered in our calculations for both atoms described by the block.

The explicit forms for new Hamiltonian matrix elements can be easily obtained from (1.14) by the means of substitution

$$\mathbf{R}_j \to \mathbf{R} = \mathbf{R}_j + \mathbf{R}_\alpha - \mathbf{R}_\beta\,,$$

which gives the relative position of the two atoms after taking into account their distinct positions $\mathbf{R}_\alpha, \mathbf{R}_\beta$ within the unit cell.

Prescriptions for the matrix elements are then

$$H_{(m,\beta),(n,\alpha)}(\mathbf{k}) = \sum_j \exp[i\mathbf{k}\cdot\mathbf{R}] \int d^3r \phi^*_{m,\beta}(\mathbf{r}) H \phi_{n,\alpha}(\mathbf{r} - \mathbf{R})\,. \tag{1.17}$$

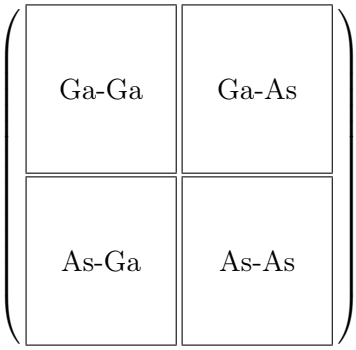

(1.18)

Figure 1: Factorization of the Hamiltonian

1.4 Approach of Slater and Koster

Further, we adopt the two-center approximation of Slater and Koster [5] and assume that in evaluating the integral

$$\int d^3r \phi^*_{m,\beta}(\mathbf{r}) H \phi_{n,\alpha}(\mathbf{r}-\mathbf{R}) \,, \tag{1.19}$$

usually referred to as a "hopping integral", we can neglect presence of everything but the atoms located at $\mathbf{R}_\beta$ and $\mathbf{R}_j + \mathbf{R}_\alpha$.

In this approach, we neglect the effect of other atoms, making the calculation similar to the calculation of a single diatomic bond, because after this approximation the value of the calculated integral depends only on vector $\mathbf{R}$ and types of atoms and orbitals involved.

As basis wavefunctions, Slater and Koster took wavefunctions with angular dependence being that of real spherical harmonics — their unnormalized prescriptions without the spherically symmetric factors are summarized in the Table 1 [6]. For reasons that will become apparent shortly we will use the same set of wavefunctions.

p orbitals	d orbitals
x, y, z	$xy, yz, zx, x^2-y^2, 3z^2-r^2$

Table 1: Basis wavefunctions

We mark integrals such as (1.19) by a symbol $E_{x,xy}(\alpha, \beta, \mathbf{R})$, meaning an integral in which the function $\phi_{n,\alpha}$ is a p_x-like function and $\phi_{m,\beta}$ is a d_{xy}-like function.

Slater and Koster found out that it is to a great extent legitimate to express all $E_{i,j}$ in terms of a small number of scalar functions $V_{i,j,Q}(\alpha, \beta, R)$ and direction cosines

$$\begin{aligned} l &= \frac{\mathbf{R}_x}{R} \\ m &= \frac{\mathbf{R}_y}{R} \\ n &= \frac{\mathbf{R}_z}{R}\,. \end{aligned} \tag{1.20}$$

For example, according to the Slater and Koster,

$$E_{x,xy}(\alpha, \beta, R, l, m, n) = \sqrt{3} l^2 m V_{p,d,\sigma}(\alpha, \beta, R) + m(1 - 2l^2) V_{p,d,\pi}(\alpha, \beta, R)\,. \tag{1.21}$$

The other conversion relations can be found in the original article [5].

It can be shown from symmetry arguments that $E_{i,j} = \pm E_{j,i}$, with minus sign used in cases, where exactly one of i, j orbitals has odd parity [1].

Possible values of Q are:

- σ for hopping integrals involving s orbital
- σ, π for hopping integrals involving p–p and p–d bonds
- σ, π, δ for hopping integrals between two d orbitals.

Using coefficients $V_{i,j,Q}$ brings about one vital simplification in that we no longer need to know the correct shape of wavefunctions ϕ. Once the set of scalar functions V is known, we can evaluate integrals (1.19) routinely and very quickly, without any reference to the precise shape of atomic wavefunctions.

Various authors postulated various dependences of V on R, in our calculations we will use a Harrison's power law dependence [7]

$$V_{i,j,Q}(\alpha, \beta, R) = C \cdot R^{-\kappa}\,, \tag{1.22}$$

where C, κ are functions of α, β, i, j, Q.

A comment must be made about the way these V are found in praxis [8, 9, 10]: As was already mentioned, one generally postulates a functional shape of dependence of V on distance, with a certain number of free parameters, and then chooses a number of physical quantities — usually important band energies in highly symmetrical points of Brillouin zone — which he wants to reproduce. After that he tries to choose the values of parameters so that algorithm given above produces results as much compatible with experimental results (or results obtained with ab-initio methods), as possible. Obtained parameters can then be used as interpolation parameters to describe the band structure throughout the

whole Brillouin zone. The value of these parameters lies in the fact that they are frequently transferable from one structure to another. They can also be used to obtain properties of structures which were not considered during the fitting of the parameters [3].

Finally, we know that interaction between two atoms diminishes quickly with their mutual distance. In mathematical terms, this can be stated in a way that integral (1.19) is a decreasing function of R. Therefore, it is sufficient to include only a finite number of terms into the sum (1.17), which corresponds to neglecting interactions between too distant atoms.

In praxis, we consider only a small number of nearest neighbours, precise number depending on the material and structure. This is one of the places, where transition from nonorthogonal wavefunctions ψ to orthogonal ϕ could cause problems, because the Löwdin functions are spread wider into space and we must in general include more neighbours than when using original atomic wavefunctions.

1.5 The onsite energies

The prescription (1.17) states that to obtain the elements of the Hamiltonian we must add contributions from atoms positioned at various positions $\mathbf{R}$, which corresponds to including contributions from different cells.

In previous part we had tactfully held back the fact that the Slater-Koster machinery for evaluating the sum in (1.17) can not be used for obtaining the terms with $\mathbf{R}_j = 0$ in diagonal blocks (with $\alpha = \beta$). In this case we have $\mathbf{R} = 0$ and calculate an "interaction" of an atom with itself, which is of a different nature than interaction between orbitals of atoms on different sites. Therefore, building up the diagonal blocks splits up into two parts — summing contributions from neighbouring atoms (with $\mathbf{R} \neq 0$) in the way proposed by Slater and Koster and evaluating contributions from terms with $\mathbf{R} = 0$. In this and following sections, we take a deeper look at these later contributions, referred to as "onsite terms".

The onsite terms have prescription

$$H^{\text{onsite}}_{(m,\alpha),(n,\alpha)} = \int d^3r \phi^*_{m,\alpha}(\mathbf{r}) H \phi_{n,\alpha}(\mathbf{r})\,. \tag{1.23}$$

However, when considering orthogonal case with S equal to unity, we can use (1.15) and write this term as

$$H^{\text{onsite}}_{(m,\alpha),(n,\alpha)} = \int d^3r \psi^*_{m,\alpha}(\mathbf{r}) H \psi_{n,\alpha}(\mathbf{r})\,. \tag{1.24}$$

Under the two center approximation, in the sum of potentials in full Hamiltonian (1.1), only the potential coming from the atom in question, $V(\mathbf{r})$, is important.

Then

$$H^{\text{onsite}}_{(m,\alpha),(n,\alpha)} = \int d^3r \psi^*_{m,\alpha}(\mathbf{r}) \left(-\frac{\hbar^2}{2M_e}\Delta + V(\mathbf{r}) \right) \psi_{n,\alpha}(\mathbf{r}) = \delta_{mn}\varepsilon_{n,\alpha}\,, \qquad (1.25)$$

where we used known solution to the atomic problem (1.2) and orthogonality of the atomic wavefunctions $\psi_{n,\alpha}$.

Thus we have shown that contribution of the onsite terms into the sum in (1.17) is accomplished by altering the values on the diagonal of the Hamiltonian matrix H. Values of the "onsite energies" $\varepsilon_{n,\alpha}$ used in tight binding are typically included as additional free parameters during the fitting mentioned in the previous section.

1.6 Including spin-orbit coupling

All what has already been stated is valid in case we do not take electronic spin into account. In cases when the existence of spin plays an important role, as in ferromagnetic materials and GaAs, we must increase the mathematical space with which we describe the problem by doubling each orbital, considering it once as having spin up and once as having spin down.

Practically it means that we must take twice as large matrices, label each matrix element with a third index, denoting spin state either "up" or "down", [5] and decide about the changes that taking spin into account produces in setting up matrix elements.

We will for simplicity assume that hopping integrals are zero between two orbitals with opposite spins, with the single exception of the onsite term. This assumption can be understood in a way that there is no spin dependent interaction between two distinct atoms. The correction made on onsite terms will represent spin orbit coupling and correction due to exchange interaction.

We have already shown in the previous section that when doing orthogonal tight binding calculations, the effective Hamiltonian used in calculating onsite terms in (1.25) is equal to the atomic Hamiltonian from (1.2). Therefore, under the assumptions presented, incorporating spin-dependent effects is provided by using a spin-dependent Hamiltonian in calculating the onsite terms.

First, let's take a look at the spin-orbit coupling. In this case, we must add the term [11]

$$H_{\text{SO}} = \lambda S \cdot L \qquad (1.26)$$

[5] We will follow common praxis and describe spin states by their projections to the z axis.

into the effective onsite Hamiltonian, making it

$$H_{\text{eff}} = -\frac{\hbar^2}{2M_e}\Delta + V(\mathbf{r}) + \lambda S \cdot L\,. \tag{1.27}$$

Here, S is operator of spin, L is operator of angular momentum and λ is a material constant. In this section, we will suppress the index denoting the atom, keeping in mind that the material constants such as λ are dependent upon the atom. We will also focus our attention exclusively on the Hilbert space spanned by the wavefunctions of the orbitals of the atom in question, because only these play role in evaluating corresponding onsite terms. In this sense it should be clear, what operators are meant under S and L in (1.26) and (1.27).

We know [6] that neither of the operators in (1.26) changes the value of the L^2, square of the orbital momentum operator. That means that H_{SO} is nonzero only between states of the same L^2, it connects p states with p states and d states with d states only. The spin-orbit does not affect s states, because s states are states of zero orbital momentum and operator in (1.26) vanishes when applied to these states. We will treat p and d states separately, the p states first:

In the basis of spherical harmonics

$$\begin{aligned} Y_{1,1} &= -\sqrt{\frac{3}{8\pi}}\frac{x+iy}{r} \\ Y_{1,0} &= \sqrt{\frac{3}{4\pi}}\frac{z}{r} \\ Y_{1,-1} &= \sqrt{\frac{3}{8\pi}}\frac{x-iy}{r} \end{aligned} \tag{1.28}$$

the angular momentum matrices[6] are equal to [6]

$$\begin{aligned} L_x &= \frac{\hbar}{\sqrt{2}}\begin{pmatrix} 0 & 1 & 0 \\ 1 & 0 & 1 \\ 0 & 1 & 0 \end{pmatrix} \\ L_y &= \frac{\hbar}{\sqrt{2}}\begin{pmatrix} 0 & -i & 0 \\ i & 0 & -i \\ 0 & i & 0 \end{pmatrix} \\ L_z &= \hbar\begin{pmatrix} 1 & 0 & 0 \\ 0 & 0 & 0 \\ 0 & 0 & -1 \end{pmatrix}. \end{aligned} \tag{1.29}$$

From (1.28) we see that wavefunctions with desired symetries of x, y, z are related with $Y_{1,i}$ through equalities

$$p_x = \frac{1}{\sqrt{2}}\left(Y_{1,-1} - Y_{1,1}\right)$$

[6] In the matrices we for simplicity supress the subspaces corresponding to s and d states, which are intact under the action of the operator under consideration.

$$\begin{aligned} p_y &= \frac{i}{\sqrt{2}}\left(Y_{1,-1}+Y_{1,1}\right) \\ p_z &= Y_{1,0}\,. \end{aligned} \tag{1.30}$$

Therefore, the transition matrix from the p_x, p_y, p_z basis to the $Y_{1,i}$ is

$$T = \frac{1}{\sqrt{2}}\begin{pmatrix} -1 & i & 0 \\ 0 & 0 & \sqrt{2} \\ 1 & i & 0 \end{pmatrix} \tag{1.31}$$

and its Hermitian conjugate is

$$T^\dagger = \frac{1}{\sqrt{2}}\begin{pmatrix} -1 & 0 & 1 \\ -i & 0 & -i \\ 0 & \sqrt{2} & 0 \end{pmatrix}\,. \tag{1.32}$$

In the p_x, p_y, p_z basis the orbital momentum operators matrices are equal to

$$\begin{aligned} L'_x &= T^\dagger L_x T = \hbar\begin{pmatrix} 0 & 0 & 0 \\ 0 & 0 & -i \\ 0 & i & 0 \end{pmatrix} \\ L'_y &= T^\dagger L_y T = \hbar\begin{pmatrix} 0 & 0 & i \\ 0 & 0 & 0 \\ -i & 0 & 0 \end{pmatrix} \\ L'_z &= T^\dagger L_z T = \hbar\begin{pmatrix} 0 & -i & 0 \\ i & 0 & 0 \\ 0 & 0 & 0 \end{pmatrix}\,. \end{aligned} \tag{1.33}$$

The operators of spin can be represented by halves of Pauli spin matrices,

$$\begin{aligned} S_x &= \frac{1}{2}\begin{pmatrix} 0 & 1 \\ 1 & 0 \end{pmatrix} \\ S_y &= \frac{1}{2}\begin{pmatrix} 0 & -i \\ i & 0 \end{pmatrix} \\ S_z &= \frac{1}{2}\begin{pmatrix} 1 & 0 \\ 0 & -1 \end{pmatrix}\,. \end{aligned} \tag{1.34}$$

We know that the mathematical space of our problem is equal to direct product of a three dimensional space spanned by linear combinations of p_x, p_y, p_z and a two dimensional space spanned by vectors representing both spin orientations. We know that S, L operators act exclusively on their respective subspaces and

therefore the calculation of the scalar product in (1.26) leads to [7]

$$H_{\mathrm{SO}} = \frac{\hbar\lambda_p}{2}\begin{pmatrix} 0 & -i & 0 & 0 & 0 & 1 \\ i & 0 & 0 & 0 & 0 & -i \\ 0 & 0 & 0 & -1 & i & 0 \\ 0 & 0 & -1 & 0 & i & 0 \\ 0 & 0 & -i & -i & 0 & 0 \\ 1 & i & 0 & 0 & 0 & 0 \end{pmatrix} \begin{matrix} p_x\uparrow \\ p_y\uparrow \\ p_z\uparrow \\ p_x\downarrow \\ p_y\downarrow \\ p_z\downarrow \end{matrix} \tag{1.35}$$

For d orbitals, we can proceed in direct analogy:
This time, spherical harmonics are

$$\begin{aligned} Y_{2,2} &= \sqrt{\frac{15}{32\pi}}\frac{(x+iy)^2}{r^2} \\ Y_{2,1} &= -\sqrt{\frac{15}{8\pi}}\frac{(x+iy)z}{r^2} \\ Y_{2,0} &= \sqrt{\frac{15}{16\pi}}\frac{3z^2-r^2}{r^2} \\ Y_{2,-1} &= \sqrt{\frac{15}{8\pi}}\frac{(x-iy)z}{r^2} \\ Y_{2,-2} &= \sqrt{\frac{15}{32\pi}}\frac{(x-iy)^2}{r^2} \end{aligned} \tag{1.36}$$

and in this basis can angular momentum operators be represented by matrices [6]

$$\begin{aligned} L_x &= \hbar\begin{pmatrix} 0 & 1 & 0 & 0 & 0 \\ 1 & 0 & \sqrt{\frac{3}{2}} & 0 & 0 \\ 0 & \sqrt{\frac{3}{2}} & 0 & \sqrt{\frac{3}{2}} & 0 \\ 0 & 0 & \sqrt{\frac{3}{2}} & 0 & 1 \\ 0 & 0 & 0 & 1 & 0 \end{pmatrix} \\ L_y &= \hbar\begin{pmatrix} 0 & -i & 0 & 0 & 0 \\ i & 0 & -i\sqrt{\frac{3}{2}} & 0 & 0 \\ 0 & i\sqrt{\frac{3}{2}} & 0 & -i\sqrt{\frac{3}{2}} & 0 \\ 0 & 0 & i\sqrt{\frac{3}{2}} & 0 & -i \\ 0 & 0 & 0 & i & 0 \end{pmatrix} \\ L_z &= \hbar\begin{pmatrix} 2 & 0 & 0 & 0 & 0 \\ 0 & 1 & 0 & 0 & 0 \\ 0 & 0 & 0 & 0 & 0 \\ 0 & 0 & 0 & -1 & 0 \\ 0 & 0 & 0 & 0 & 2 \end{pmatrix}. \end{aligned} \tag{1.37}$$

[7] After the matrix we denoted, which state corresponds to the given row (and corresponding column) of the matrix.

Going through the same calculations as in the case of p orbitals, we get[8]

$$H_{\mathrm{SO}} = \frac{\hbar\lambda_d}{2} \begin{pmatrix} 0 & 0 & 0 & 2i & 0 & 0 & 1 & -i & 0 & 0 \\ 0 & 0 & i & 0 & 0 & -1 & 0 & 0 & -i & -i\sqrt{3} \\ 0 & -i & 0 & 0 & 0 & i & 0 & 0 & -1 & \sqrt{3} \\ -2i & 0 & 0 & 0 & 0 & 0 & i & 1 & 0 & 0 \\ 0 & 0 & 0 & 0 & 0 & 0 & i\sqrt{3} & -\sqrt{3} & 0 & 0 \\ 0 & -1 & -i & 0 & 0 & 0 & 0 & 0 & -2i & 0 \\ 1 & 0 & 0 & -i & -i\sqrt{3} & 0 & 0 & -i & 0 & 0 \\ i & 0 & 0 & 1 & -\sqrt{3} & 0 & i & 0 & 0 & 0 \\ 0 & i & -1 & 0 & 0 & 2i & 0 & 0 & 0 & 0 \\ 0 & i\sqrt{3} & \sqrt{3} & 0 & 0 & 0 & 0 & 0 & 0 & 0 \end{pmatrix} \begin{matrix} d_{xy}\uparrow \\ d_{yz}\uparrow \\ d_{zx}\uparrow \\ d_{x^2-y^2}\uparrow \\ d_{3z^2-r^2}\uparrow \\ d_{xy}\downarrow \\ d_{yz}\downarrow \\ d_{zx}\downarrow \\ d_{x^2-y^2}\downarrow \\ d_{3z^2-r^2}\downarrow \end{matrix} \tag{1.38}$$

1.7 Exchange interaction

Procedure described above was derived using independent electron approximation. However, ferromagnetism follows from interactions between various electrons in the solid. Therefore, it is impossible to describe ferromagnetic materials faithfully by means of the algorithm mentioned above. The situation can be improved by taking exchange energy into account.

Majority of electrons in ferromagnetic materials have spins aligned in a specific direction, which gives rise to a nonzero magnetization [12]. In such material, it is energetically favourable for an electron to have spin oriented in the direction of magnetization, because in such case the magnitude of the negative exchange energy of the many-electron system is maximized. In ferromagnets, the kinetic energy penalty for aligning spins is smaller than the magnitude of the gained exchange energy and, therefore, the magnetically ordered state minimizes the total energy of the system [6]. For that reason we introduce constant M, equal to the single-particle energy difference between spin up and down states of an electron placed on a specific orbital.[9]

If we assume that the splitting of the energy levels is symmetric under the influence of the exchange interaction, then we can write the contribution of the exchange interaction into the Hamiltonian as

$$H_F = M\mathbf{n}\cdot S\,. \tag{1.39}$$

Here $\mathbf{n}$ is a unit vector in the direction of magnetization and S is the operator of spin.

[8] For greater generality, we permitted various coupling constants for p and d orbitals.

[9] The value of M will of course depend on the choice of orbital.

If the magnetization is oriented in the direction of the positive z axis, then this expression is valid, because it tells us to alter the energies of electrons in orbitals with opposite S_z projections to maintain an energy difference M. It is consistent with the information provided in previous paragraphs, because these states represent at the same time pure states of spin in the direction of magnetization. General validity of this expression is then ascertained by the scalar nature of the addend, which transforms well under rotations.

We will describe the direction of magnetization by spherical angles ϕ, θ, with unit vector $\mathbf{n}$ having components

$$\begin{aligned} n_x &= \sin\phi\cos\theta \\ n_y &= \sin\phi\sin\theta \\ n_z &= \cos\phi\,. \end{aligned} \tag{1.40}$$

After adopting this convention, the terms added to the Hamiltonian to describe the exchange interaction have a form

$$H_F = M \begin{pmatrix} \cos\phi & \sin\phi\ e^{-i\theta} \\ \sin\phi\ e^{i\theta} & -\cos\phi \end{pmatrix}. \tag{1.41}$$

1.8 Layered materials

When coming to layered materials, [10] majority of the things we have stated in previous sections remains unchanged, the only difference inheres in that we lose periodicity in the direction of growth, in the direction perpendicular to the layers. From now on, we will refer to this direction as to the direction of the z axis.

We assume that periodicity in x and y directions remains maintained. In such case we have only two primitive vectors, both lying in the xy plane, which gives rise to a two dimensional primitive cell in this plane. However, in dealing with layered materials, the most important concept is a semi-infinite three dimensional prism, formed when we stretch the 2-D unit cell in the z direction into both infinities. This prism has two properties that make it especially appealing for the description of the layered systems:

- It reflects the underlying two dimensional periodicity.
- We can perceive the prism as a fundamental cell, from which all the space can be put together.

[10] Materials, in which atoms are positioned in mutually parallel planes. In each one of these planes the atoms are distributed 2-D periodically, but the properties of periodicity can differ between layers (for example, lattice constants can be different in different layers).

Both properties make the prism closely analogous to the ordinary unit cell in the problem with a three dimensional translational periodicity.

The problem of building a physically relevant Hamiltonian can be solved in a complete analogy with the systems discussed in previous sections. First, we have to choose a correct 2-D unit cell to start with. We have to pay a careful attention to this choice, because we must ensure that all layers are periodical with respect to this 2-D unit cell. From this cell, we make up a semi-infinite prism by the procedure described above. As the atoms of the basis[11] we then have to take all atoms that appear in the prism.

For each such atom, we must add corresponding terms into the Bloch sum (1.16). In the language of matrices it means that for each such atom, we must allocate appropriate number of rows, precise number given by the number of orbitals of the atom. The equations (1.8), (1.13) remain pivotal, the elements of matrices obtained according to the prescription (1.17), with indices α, β running over atoms in the prism. To evaluate these matrix elements, we again use the method of Slater and Koster. This way we formally unify the procedures used in calculating properties of both layered and fully crystalline materials.

One technical comment about interpretation should be stressed out — because of the transational invariance present in the x and y directions only, the underlying Brillouin zone is two dimensional and the $\mathbf{k}$ vector has only two components. It could appear that we could get mathematically into trouble while making the scalar product of a two dimensional vector $\mathbf{k}$ with three dimensional position vectors $\mathbf{R}$ in (1.17). This obstacle can be avoided by defining the $\mathbf{k}$ vector to be three dimensional, with third component identically equal to zero. We then arrive at the correct Bloch sums (1.16) and therefore obtain sensible results.

1.9 Schottky Barrier

When we put two materials together to create a common interface, a charge flow will occur from one material to the other, because of different positions of Fermi levels in both materials. This movement of charge gives rise to an additional electric potential in the vicinity of the interface and this potential must be added into the Hamiltonian (1.1) [13].

In our case, on the interface between a metal and a semiconductor, we will assume that the contact with semiconductor does not give rise to an additional electrical potential in the metal. It is ensured by the great mobility of the free electrons in the metal [7], which effectively screens any inner electric field. In the semiconductor, the screening is much weaker due to the small concentration of free

[11] Which correspond to different α in (1.17).

carriers, which gives rise to a nontrivial potential. For an n-type semiconductor, the additional potential is positive, its value is highest at the surface and then decreases with the increased distance from the interface [13].

This potential can be easily taken into account by altering the values of the onsite energies. This change in the onsite energies is considered to depend only on the position of the atom, not on the type of the atom or the type of the orbital.

In our calculations we use a trapezoidal model of Schottky barrier, with the linear dependence of the energy change on the distance D from the interface,

$$\Delta\varepsilon_{\text{onsite}}(D) = C_1 + C_2 D \tag{1.42}$$

in an appropriately chosen range of D. This range must be chosen so that the change of the onsite energies in the metal part of the Hamiltonian is zero.

Special cases of this model are rectangular and triangular barriers. It can also be used as an approximation to the real shape of the barrier in cases when the number of layers included into the calculations is far smaller than the real thickness of the Schottky barrier, which will be our case.

1.10 Algorithm

We can summarize the procedure of the tight binding calculation into a neat algorithm:

- Find a unit cell of the material, either 2-D or 3-D.
- Find out, how many atoms are present in the unit cell.[12]
- For each such atom, decide which orbitals are physically relevant for the problem and should be used.
- When calculating Hamiltonian matrix corresponding to wavevector $\mathbf{k}$, first add the onsite terms — energies $E_{n,\alpha}$, spin-orbit coupling and the exchange interaction part (if applicable).
- When calculating interface between a metal and a semiconductor, add contribution corresponding to the Schottky barrier.
- Based on the parameters available and the structure of the material, decide how many terms will be included into the sum (1.17) in dependence on various indices m, n, α, β.

[12] In the case of layered material, we mean in the unit cell stretched into infinities in z direction.

- Evaluate the sums in (1.17) with the use of Slater-Koster approach and add them into Hamiltonian.
- Calculate the overlap matrix elements (1.7), if necessary.
- Solve the full eigenvalue equation (1.8) or secular equation (1.13) to obtain corresponding electron energies and eigenvectors.

Chapter 2

Computer Program

2.1 Basic description

The computer program was written in the programming language Fortran, its source code can be found on the enclosed CD.

It can perform two types of calculations. If a set of vectors in reciprocal space is provided on the input, the program calculates the eigenenergies $E_n(\mathbf{k})$ of the corresponding equation (1.8) or (1.13). This feature can be used to obtain electronic band structures of materials, for which tight binding parameters are available.

The more substantial value of the program lies in its ability to calculate integrated quantities, such as densities of state (DOS) or total energy (TOTE). The most general quantities that can be computed with the program are quantities expressible in the form

$$\begin{aligned} I(\varepsilon) &= \frac{1}{V_{B.Z}} \sum_n \int_{B.Z.} d\mathbf{k}\, f_n(\mathbf{k})\, \delta(\varepsilon - \varepsilon_n(\mathbf{k})) \\ J(\varepsilon) &= \frac{1}{V_{B.Z}} \sum_n \int_{B.Z.} d\mathbf{k}\, f_n(\mathbf{k})\, \theta(\varepsilon - \varepsilon_n(\mathbf{k}))\,. \end{aligned} \tag{2.1}$$

Here f_n is some function we want to integrate and $V_{B.Z.}$ is the volume of the first Brillouin Zone. The summation goes over all eigenenergies.

By choosing $f_n = 1$, the two integrals above represent DOS and the 3D or 2D electron density [14]. The choice $f_n(\mathbf{k}) = \varepsilon_n(\mathbf{k})$ in the lower integral leads to a calculation of total energy.

Sometimes we are interested in partial values of these quantities, for example DOS coming from the s states only. In order to obtain this value, we must multiply the integrated function by a coefficient representing the projection. If we label the eigenvector corresponding to the solution $\varepsilon_n(\mathbf{k})$ as $|\xi_n(\mathbf{k})\rangle$, then the value of the

multiplication coefficient is

$$w_n(\mathbf{k}) = \langle \xi_n(\mathbf{k}) | W | \xi_n(\mathbf{k}) \rangle \,, \tag{2.2}$$

where W is a projector to states we are interested in.

During our calculations, we must construct Hamiltonian matrix and S-matrix with overlaps for numerous reciprocal vectors $\mathbf{k}$. To eliminate redundant computations, the construction of the Hamiltonian is split into two parts. In the first part, the program sets up the part of the Hamiltonian, which is independent of $\mathbf{k}$. This part contains onsite energies, spin-orbit coupling, exchange energy and the Schottky barrier. This part needs to be calculated only once.

The program then runs through the set of all $\mathbf{k}$ for which we need to know eigenenergies, completes the Hamiltonian and the S-matrix by adding the $\mathbf{k}$ dependent terms and searches for the eigenvalues and eigenvectors. Based on these eigenvalues and eigenvectors, it calculates and stores information that is necessary for further computations. This information includes the calculated eigenvalues, together with the values of integrated functions multiplied by coefficients w_n.

In our calculations, all atoms are represented by 20 orbitals — s, p, d and s* orbitals for both spin polarizations. Orbitals s* are virtual, nonexistent orbitals with spherical symmetry. They must have been added because of the parametrization used to describe GaAs. This parametrization is discussed in greater detail further.

2.2 Input parameters

One of the basic ideas underlying the program was to keep the program and the parameters describing the calculated structure as much separated, as possible. It was aimed to write a very general program that is capable to perform any tight binding calculation under the approximations mentioned in the previous section. The code was written with an emphasis on minimalization of changes necessary to implement any additional features.

The program starts by looking up the type of calculation that should be performed. There are overall four types of calculation, because three integration procedures were implemented besides the calculation of the band structure. One of them is used to evaluate integrals (2.1) over a three dimensional Brillouin zone, two distinct procedures are used to evaluate integrals over two dimensional BZ.

After calling corresponding subroutine, basic data describing the calculation are loaded. The subroutines used for integrating read information about the number of points in BZ, at which eigenenergies will be calculated, together with the range of energies, for which integral should be evaluated. All subroutines continue

by finding out the number of layers, number of distinct chemical identities present and other numbers needed to allocate sufficient amount of memory.

Then, the parameters needed to set up the onsite part of the Hamiltonian matrix are loaded and the onsite part H_0 is built up, according to the prescriptions (1.25), (1.35), (1.38), (1.41) and (1.42). The direction of magnetization was considered to be the same in all layers, because more general case was not necessary for the calculations performed. This direction is given by two polar angles which determine the magnetization direction in a specific coordinate system. For this description, we always chose the angles relative to the coordinate system in which two of the primitive vectors of the structure lie in the xy plane.

However, it would be difficult to carry out calculations of quantities connected with majority/minority spin states in this coordinate system. To get rid of this handicap, the calculations were performed in the coordinate system in which magnetization is oriented in the direction of the z axis. This is obtained by means of rotating all vectors (represented by the positions of atoms and reciprocal space vectors $\mathbf{k}$) by an appropriate rotation. Parameters of this rotation are determined from the known coordinates of the magnetization vector in the coordinate system given by the primitive vectors.

As the next step, the program gathers information about the "bond types". The concept of bond types is very tightly related to the partitioning of the Hamiltonian into blocks, mentioned earlier [1]. The Hamiltonian is constructed in a way that elements contained in the block $\alpha - \beta$ describe interactions between the atom at the position $\mathbf{R}_\beta$ and the atoms at positions $\mathbf{R}_j + \mathbf{R}_\alpha$ for various vectors $\mathbf{R}_j$ from the primitive lattice. In the previously encountered example of GaAs ($\alpha =$ Ga, $\beta =$ As) it means between a Ga atom and all As atoms within the range of the interaction. Because this range is taken to be finite, we do not consider contributions from all possible $\mathbf{R}_j$, but only from a limited number of them. Therefore, the set of $\mathbf{R}$ for which we evaluate term

$$\exp[i\mathbf{k} \cdot \mathbf{R}] E_{m,n}(\alpha, \beta, \mathbf{R}) \tag{2.3}$$

from (1.17) is finite. To be able to evaluate (2.3) for all $\mathbf{k}$, we must store information about the vectors $\mathbf{R}$, refferred to as "positions of nearest neighbours", and respective values of $E_{m,n}$. These two pieces of data, together with information about elements of S-matrix [2], comprise the contents of an abstract quantity "bond type". The concept of bond type is especially useful in cases of layered materials with large numbers of layers, as will become clear shortly.

To obtain for each bond type a set of vectors giving the positions of nearest neighbours, a specific procedure which serves as a data bank of commonly used

[1] See Figure 1 and related text in the first chapter.

[2] We assumed that elements of this matrix can be obtained through the analogous set of rules, as the elements of the Hamiltonian (example of these is (1.21)).

sets of nearest neighbours is used.[3] Each encountered set of nearest neighbours was numbered[4] and the input file then references these sets of vectors with the help of this numbering. Additional information must be provided to obtain a correct physical scaling of the vectors. In the end, the vectors are rotated to transform their coordinates into the system in which magnetization has the direction of the z axis.

Calculation of coefficients $E_{m,n}$ is performed in two steps. First, the values of scalar functions $V_{i,j,Q}(\alpha, \beta, R)$ are determined for all i, j, Q and vectors $\mathbf{R}$. In the program, various ways to calculate these values are implemented, some of them will be touched on further. The coefficients $E_{m,n}$ are then obtained by the means of Slater-Koster rules, such as (1.21).

In the end, subroutines used for integration load data about the functions f_n that should be integrated. The program distinguishes between various functions in the same way it determines which positions of nearest neighbours should it use — each function is given an index, through which it can be singled out. This is convenient due to the small class of functions which we typically want to integrate. In case we needed to integrate a previously unencountered function, a corresponding passage can be easily added into the source code. We implemented an option to calculate partial values of integrated quantities, currently it is possible to make no projection at all ($w_n(\mathbf{k}) = 1$) or to project to all orbitals belonging to a single atom as well as orbitals belonging to a sequence of atoms. More specialized projections, such as DOS coming from the d states on Ga atoms, can be reached by choosing f_n to be projector to the d states and then projecting the result to gallium atoms by an appropriate choice of w_n.

2.3 Constructing the Hamiltonian, calculating eigenvalues

As was mentioned in the previous section, the construction of the Hamiltonian is split into two parts. During the procedure of reading the input file, we construct the onsite part of the matrix, as well as obtain positions of nearest neighbours and calculate respective Slater Koster coefficients $E_{m,n}$.

When calculating the band structure, the set of reciprocal space vectors $\mathbf{k}$, for which we want to set up the Hamiltonian, is provided in a separate input file. In integration procedures, the vectors $\mathbf{k}$ are chosen so that they fill the first Brillouin zone evenly.

[3] This approach is taken from Jan Mol's unpublished results [15].

[4] The set of first neighbours in BCC structure is given number 2, the set of first neigbhours in FCC structure is given number 3, ...

For each of these vectors,[5] contributions according to the formula (1.17) are added into the Hamiltonian matrix, which is already filled with the pre-calculated **k**-independent part.

If we define the matrix $B(\alpha, \beta, \mathbf{R}_0)$ to have elements $E_{m,n}(\alpha, \beta, \mathbf{R}_0)$, then the formula (1.17) tells us that addend we must add to the block $\alpha - \beta$ in the Hamiltonian is equal to

$$\sum_{\mathbf{R}} \exp(i\mathbf{k} \cdot \mathbf{R}) B(\alpha, \beta, \mathbf{R}) \,, \tag{2.4}$$

with sum going over all nearest neighbours considered in our model. The matrices $B(\alpha, \beta, \mathbf{R})$ are independent of **k** and can be pre-calculated.

The existence of matrices B shows to be especially valuable in case two blocks possess the same sets of nearest neighbours **R** and matrices B, because the sum (2.4) needs to be calculated only once and the result can then be used in both these blocks. This situation of two blocks being described by a single "bond type" typically arises in the case of layered materials with a large number of layers. For example, in layered GaAs, the interaction between Ga atom on third layer and As atom on fourth layer is in our model exactly the same, as the interaction between Ga atom on eighth layer and As atom on ninth layer. This fact manifests itself in that both corresponding blocks in the Hamiltonian have the same contents, a notion we formalized by defining the bond type and B matrices.

The concept of bond type is utile, because it saves computer time and can also be conveniently used for the description of the material in the input file. For each block we just enter the number of the bond type that describes this block and then define the bond types on a different part of the input file.

The matrix with overlaps is, in case we want it to be considered, calculated in absolutely analogous manner as the matrix corresponding to the Hamiltonian. The only difference to be stressed out is the fact that during the construction of the S-matrix, we do not add the onsite part. Instead, we add unity to all diagonal elements. This addition corresponds to including an overlap of the orbital with itself, which by definition is equal to one.

After having complete Hamiltonian and the S-matrix, the solution to one of the equations (1.13) or (1.8) is searched for, both eigenvalues and eigenvectors. For this, routines ZHEGV and ZHEEV of the standard LAPACK package are used [16].

When performing integration, we calculate values of integrated functions at each **k**, multiplied by the projection coefficients w_n. These values, together with the values of calculated electron energies E_n then serve as an input for the integration procedures.

[5] Before making any calculations with them, they are rotated into the coordinate system we are working in.

2.4 Integration

Subroutines used for integration were originally written by J. Mol and T. Jungwirth [15, 17]. The original codes were modified and generalized during the writing of the program. All integration subroutines can be used for cubic/square Brillouin zones only.

For integration in the three dimensional reciprocal space, classical tetrahedron method [18] is used. In this method, the first Brillouin zone is divided into evenly big cubes and each cube is then divided into tetrahedra. The contribution from each tetrahedron is calculated, these contributions are then summed together and the result is then normalized by a suitably chosen factor. In our calculations, we chose normalization per atom of the unit cell.

As we know from the prescription (2.1), the integration over each tetrahedron is repeated, the number of repetitions is given by the dimension of the Hamiltonian matrix.

The values of the energies E_n and functions f_n are interpolated linearly inside each tetrahedron between their values at the vertices of the tetrahedra. Then it is possible to obtain an analytical prescription for the value of the integral over the tetrahedron in terms of these vertex values. This prescription can be found for example in the article reference.

For evaluation in the two dimensions, two distinct methods can be used. The first one, the triangular method [14], is an adaptation of the tetrahedron method for the two dimensional Brillouin zone. It is based on the same principles — the Brillouin zone is divided into triangles, quantities used in calculations are linearly interpolated between the values at the vertices and then an analytical formula is employed.

The other method is based on replacing the step function and Dirac delta function by functions

$$\begin{aligned} \theta(x) &\rightarrow \frac{1}{2} + \frac{1}{\pi} \arctan \frac{x}{\epsilon} \\ \delta(x) &\rightarrow \frac{1}{\pi} \frac{\epsilon}{x^2 + \epsilon^2}, \end{aligned} \tag{2.5}$$

where ϵ is a parameter of the calculation. In the limit $\epsilon \rightarrow 0^+$ both functions on the right converge to the functions on the left in the sense of distributions.

After this replacement, we can use a two dimensional analogy of the trapezoidal rule for the integration [19]. It involves taking a weighted sum of the function values in the points evenly distributed over the integrated area (the first Brillouin zone). The weights are set so that corners of the Brillouin zone are prescribed weight equal to one, the other points on the edges have weight two and the points in the interior are given weight four. This way we can also calculate the integrals (2.1).

However, the applicability of this method to obtain values of integrals $I(\varepsilon)$ is doubtful, because of the role of the parameter ϵ. In the limit $\epsilon \to 0^+$ we get zero, because the energies in the vertices will generally have energies different from the energy, for which we evaluate $I(E)$. If we on the other hand take ϵ to be too big, the replacements we made for the delta distribution (2.5) will not be a very reliable approximation. Because of this, the method using approximations (2.5) was not used in obtaining the results presented in this work.

Chapter 3

GaAs, Fe and Tests to the Program

3.1 Gallium arsenide

The first calculations were performed on the bulk GaAs. Gallium arsenide crystallizes in the cubic zinc blende structure, which can be perceived as two penetrating FCC lattices. Therefore, as the unit cell of the material we can take the unit cell of the FCC lattice made up by gallium atoms. In each such unit cell, there is one gallium atom and one arsenic atom; therefore, we have a material with two atoms in the unit cell.

In our calculations we used the parametrization[1] of Jancu et al. [8]. Their tight binding model is based on ten orbitals $(s; x, y, z; xy, yz, zx, x^2 - y^2, 3z^2 - r^2; s^*)$ per atom. The orbital s^* with spherical symmetry was added to account for higher energy levels that are not an explicit part of the calculations. These orbitals do not represent real orbitals, but were included to improve the results obtained by the model. The parametrization includes the constants λ giving the strength of the spin orbit coupling, we therefore double each orbital to account for both spin states. In grand total, the two atoms in the unit cell are represented by twenty orbitals each. No exchange splitting was considered, the orbitals are chosen to be Löwdin orbitals (orthogonal tight binding). The functions V were chosen to follow the scaling law (1.22), values of coefficients C and κ are stated in the Jancu's article.

Of all the parametrization encountered, this parametrization contained the

[1] Under "parametrization" we mean the set of orbitals used for atoms, values of on-site energies, spin orbit coupling constants, strength of the exchange interaction and the prescription to calculate $V_{i,j,Q}$.

largest set of orbitals. Because sets of orbitals with which all other parametrizations work constituted a subset of this large set, we decided to write the program in a way that all atoms are represented by the twenty orbitals given above. In case that in any of the parametrizations there is an atom with one or more orbitals that are not included (typically s^*), we can exclude it from the calculations by setting corresponding hopping integrals $V_{i,j,Q}$ equal to zero. Because awkward choice of corresponding onsite energies could alter the results of integrations, it is necessary to place these energies above the largest energy for which we calculate integrals (2.1). If, however, we choose ε_{s^*} to be too big, it becomes the largest eigenvalue of the matrix H, due to zero value of coefficients $V_{i,s^*,\sigma}$. This choice would then decrease the accuracy of our calculations, which is given by the largest eigenvalue of H [16].

Only the interaction between nearest neighbours was considered, these are placed at (relative) positions

$$\begin{aligned} \mathbf{R}_A &= \left(\frac{L}{4}, \frac{L}{4}, \frac{L}{4}\right) \\ \mathbf{R}_B &= \left(-\frac{L}{4}, \frac{L}{4}, \frac{L}{4}\right) \\ \mathbf{R}_C &= \left(\frac{L}{4}, -\frac{L}{4}, \frac{L}{4}\right) \\ \mathbf{R}_D &= \left(\frac{L}{4}, \frac{L}{4}, -\frac{L}{4}\right) . \end{aligned} \tag{3.1}$$

Here we stated the coordinates of neighbouring arsenic atoms with respect to the gallium atoms, L denotes the lattice constant of the material, $L = 5.6532$ Å [8]. Taking only first neighbours corresponds to restriction of the interaction range to approximately 2.5 Å.

Apart from the parametrization, the article also states several results obtained with the parameters. These results include band energies at highly symmetrical points in the Brillouin zone, reference band structure and graphs of energy dependence of DOS and several partial densities of state. By comparison of these results with results received with our program, we were able to verify its functionality.

To be specific, by these tests we verified that:

- procedure loading data about the structure works correctly
- the Hamiltonian is put together properly, especially that the Slater-Koster rules are implemented well
- the program is able to perform integrations

3.2 Iron

Iron crystallizes in BCC structure with lattice constant 2.87 Å [10].

We used two distinct parametrizations to obtain values of iron onsite energies and respective hoppings $V_{i,j,Q}$ [9, 10]. Both these parametrizations are orthogonal, i.e. they take S-matrix equal to unity, and use the two center approximation. Interaction is limited to the third nearest neighbours; each atom is represented by 18 orbitals, because the s^* orbitals are not involved. For the strength of the spin-orbit coupling in iron we used value 0.0585 eV for all orbitals, as given by the article [20]. We stress out that this spin-orbit coupling constant for Fe was obtained in a different formulation of the tight binding method so it may not be comparable with our parametrization.

The first parametrization we used can be found in the book by Papaconstantopoulos [10]. The book states values of coefficients V explicitly for the distance between first, second and third nearest neighbours for the value of lattice constant equal to 2.86057 Å. For small changes in the lattice constant, Papaconstantopoulos suggests using power law dependence (1.22) with following values of κ:

Orbitals involved in the bond	κ
s–s	1
s–p	2
s–d, p–p	3
p–d	4
d–d	5

Table 2: Scaling constants used for the parameters from [10]

This scaling law provides "very good agreement[2] for variations of the lattice constant as large as 5%".

The other parametrization we used was the parameterization by Shi and Papaconstantopoulos [9], which presents an extension to Harrison's original theory [7]. Harrison created a set of universal hopping parameters that can easily be used to perform calculations. These parameters can be divided into two groups — universal parameters, common to all elements, and parameters describing the element. The universality of the parametrization then relies on the fact that there are only three element-dependent parameters. Shi and Papaconstantopoulos found out that the predictive strength of the model can be improved vastly by increasing the number of element-dependent parameters up to five. In their article they list new universal parameters, as well as parameters for various elements. These include parameters for ferromagnetic iron, which we used.

[2] In the resulting bandstructure, when comparing to results of first-principles APW calculations.

In this model, parameters scale with the distance according to the Table 3.

Orbitals involved in the bond	κ
s–s, s–p, p–p	2
s–d, p–d	3.5
d–d	5

Table 3: Scaling constants used for the parameters from [9]

Chapter 4

Magnetic Anisotropies of Iron Layers on GaAs

4.1 Theoretical aspects

After we tested our program and calculated various properties of bulk gallium arsenide and iron, we turned our attention to investigation of properties of the iron layers on top of the GaAs(001) surface, probably the most extensively studied example of an interface between a ferromagnetic metal and a semiconductor [21]. These interfaces could play a fundamental role in constructing novel electronic devices, utilizing not only a charge of the electron, but also its spin. In our calculations we focus on the determination of the magnetic anisotropy of Fe/GaAs(001) at the Fermi level and investigation of its properties, especially dependence of uniaxial anisotropy constant K_{ui} on the number of iron layers.

From the symmetry arguments we expect the resulting anisotropy to be a superposition of twofold uniaxial and fourfold cubic in-plane anisotropy,[1] together with the contribution describing the anisotropy in the direction perpendicular to the layers. We therefore assume that the total energy density depends on the polar coordinates of magnetization according to ([22], slightly modified)

$$\begin{aligned} F(\theta,\phi) = F_0 \quad &- \quad \frac{K_c}{2}\left[\cos^4\theta + \frac{1}{4}\Big(3+\cos(4\phi)\Big)\sin^4\theta\right] - \\ &- \quad K_{ui}\sin^2(\phi-\delta)\sin^2\theta - K_{up}\cos^2\theta + \\ &+ \quad F_{\text{shape}}\cos^2\theta\,. \end{aligned} \tag{4.1}$$

Here δ is the angle between the easy axis of the twofold in-plane anisotropy with

[1] In-plane directions are the directions lying in the plane parallel to the layers of the material.

respect to the easy axis of the fourfold anisotropy and θ and ϕ are the polar and azimuthal angles of the magnetization with respect to the [001] resp. [100] direction. F_{shape} is the contribution that stems from the classical dipole-dipole interaction of the magnetic moments [23] and which rotates the magnetization into the in-plane direction. The value of F_{shape} is equal to

$$F_{\text{shape}} = \frac{1}{2}\mu_0 M_s^2\,, \tag{4.2}$$

where M_s is the saturation magnetization and μ_0 permeability of vacuum [24]. Because GaAs is non-magnetic, we expect that the contribution of GaAs layers to the shape anisotropy is negligible in comparison with the contribution of iron layers. In such case we can estimate the magnitude of shape anisotropy by using the saturation magnetization of bulk iron, which is 1717 Gauss. After taking into account the dimensions of investigated structures, then our estimate of the contribution of shape anisotropy into total anisotropy is 134.92 μeV per iron atom. This estimate is very near the real value of shape anisotropy for iron films on GaAs because experiments report that the average magnetic moment in iron layers on GaAs is bulk-like [21]. This observation was confirmed by our calculations, discussed in further detail later. Important notion about the shape anisotropy is the fact that this contribution does not enter our calculations in any place, because our simplified model does not take the dipole-dipole interaction into account. In calculating anisotropy constants from the data obtained with our program we can therefore ignore this term in expression (4.1).

To obtain the four unknown constants in (4.1), we must calculate the total energy for four distinct directions of magnetization for each investigated structure. In thin iron films on GaAs(001), strong uniaxial anisotropy with easy axis [110] is observed [22]. Therefore, we calculate total energy for the directions of magnetization [001], [010], [110] and $[1\bar{1}0]$.[2] For these directions we get free energies

$$\begin{aligned} F_{[110]} &= F_0 - \frac{K_c}{4} \\ F_{[1\bar{1}0]} &= F_0 - \frac{K_c}{4} - K_{ui} \\ F_{[010]} &= F_0 - \frac{K_c}{2} - \frac{K_{ui}}{2} \\ F_{[001]} &= F_0 - \frac{K_c}{2} - K_{up}\,. \end{aligned} \tag{4.3}$$

After calculating free energies for the four directions we can obtain the anisotropy

[2]For orientation of the coordinate axes with respect to the atoms in the vicinity of interface, see Figure 2.

constants by the means of formulae

$$\begin{aligned} K_{ui} &= F_{[110]} - F_{[1\bar{1}0]} \\ K_{up} &= F_{[001]} - F_{[010]} + \frac{F_{[110]} - F_{[1\bar{1}0]}}{2} \\ K_c &= 2F_{[110]} + 2F_{[1\bar{1}0]} - 4F_{[010]}\,, \end{aligned}$$

which are derived directly from relations (4.3).

Because we could not determine the position of Fermi energy of the system precisely, we calculated energy density and TOTE integrals[3] for equidistant set of energies separated by energy difference $\Delta\varepsilon$. From these we obtained values on the Fermi level by linear interpolation. We stress out that the position of the Fermi level, expressed via the parameter ε in (2.1), differs for the four directions of magnetization and due to the high precision demanded from our calculations this shift of Fermi level must be taken into account.

It is customary to separate the anisotropy constants into corresponding surface and volume contributions K_i^s, K_i^v in accordance with the relation [22]

$$K_i = K_i^v + \frac{K_i^s}{d} \qquad i \in \{ui, c\}\,, \tag{4.4}$$

where d is the thickness of the film. Since we consider in our calculations cubic Fe, its bulk uniaxial anisotropy is zero and we obtain only the surface contribution. For that reason we assumed $K_{ui}^v = 0$ and used formula

$$K_{ui} = \frac{K_{ui}^s}{d} \tag{4.5}$$

to fit the uniaxial anisotropy constant, instead of (4.4).

4.2 Details of computation

Before starting the calculations, we had to answer following questions concerning precise details of the computation:

- How are atoms arranged in the vicinity of the boundary?
- How do we obtain hopping parameters for Ga-Fe and As-Fe bonds?
- Which of the two iron parametrizations should we use?
- Should we add the spin-orbit coupling into iron?

[3]Integrals $J(\varepsilon)$ with $f_n = 1$ respectively ε_n.

- Should we include Schottky barrier into our model?
- What distance should we choose between the first Fe and last GaAs layers?

As of the arrangement of atoms around the interface, we assumed that the interface is perfect, with no interdiffusion of atoms across the boundary. Because of the reasonably low lattice mismatch of Fe and GaAs, we assumed that the iron adopts the value of the lattice constant of bulk gallium arsenide. The atoms in the layers nearest to the surface were taken to be distributed according to the Figure 2, which illustrates an As-terminated surface.[4] This figure shows projection of four 2D unit cells to three atomic (001) planes, these projections are displayed alongside each other and depict (from the left, in the sense of increasing z coordintae) the last two layers of GaAs and the first layer of iron film. Dashed lines circumscribe the unit cells. The same atomic configuration was used for example in [23].

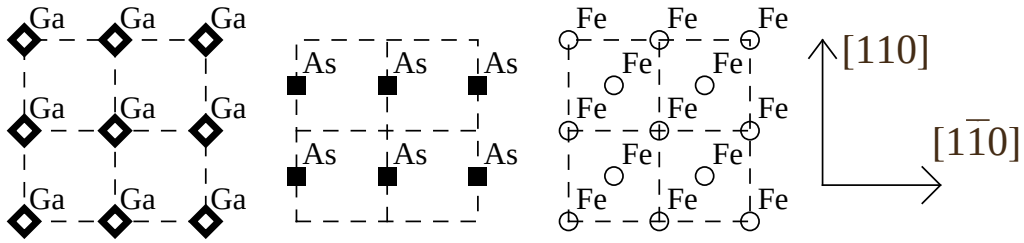

Figure 2: Distribution of atoms in the vicinity of interface.

Distribution of atoms in GaAs resp. Fe part of the structure is taken to be the same as in the bulk state i.e. zinc blende resp. BCC structure. Because we changed the in-plane dimensions of iron lattice constant, we also modified distance between adjacent iron layers. We adjusted this distance so that the volume corresponding to each iron atom in the new structure was the same as the volume per atom in the bulk iron. These modifications resulted in changes of distances between nearest neighbours in iron; however, these changes were smaller than 3 %. The distance between nearest neighbours, which has the largest influence on results, is altered by less than 1 ‰.

Gallium arsenide substrate upon which the iron was deposited was represented by 10 GaAs layers. Regarding the tight binding parameters, in gallium arsenide we used the same onsite energies as in bulk material. The onsite energies of iron were shifted in a way to ensure common Fermi level in bulk iron and bulk GaAs [25]. Hopping parameters $V_{i,j,Q}$ for Fe-Fe and Ga-As bonds were taken to be the same

[4] Ga-terminated surface looks similarly with As and Ga atoms interchanged.

as in the bulk cases, the same is true about the spin-orbit coupling constants in both materials.

To obtain the hopping integrals for Ga-Fe and As-Fe bonds, we followed common praxis [25], [26] — we first determined the values of hopping integrals between Fe sites and between Ga and As sites for the atomic distance at the interface. As hopping integral for Ga-Fe and As-Fe bonds we then took the geometric mean of these two "bulk" hopping integrals. For s-s bonds, e.g.,

$$V_{ss\sigma,\mathrm{G}a-Fe} = \sqrt{V_{ss\sigma,\mathrm{G}a-As} \cdot V_{ss\sigma,\mathrm{F}e-Fe}}\,. \tag{4.6}$$

If the corresponding hopping integrals for Fe-Fe and Ga-As bonds had opposite signs, we set hopping integral zero. Between Fe and GaAs we introduced interaction between first neighbours only, taking into account the range of interaction between atoms in bulk GaAs.

To decide which set of iron parameters should be used, as well as whether the spin orbit in iron and Schottky barrier should be explicitly inserted into our model, we performed a series of tests. The inclusion of iron spin-orbit coupling is somewhat controversial, because theoretical models [23] indicate that magnetic anisotropies, which we were interested in, rely on the value of spin-orbit coupling constant. On the other hand, the iron parameters we used were not optimized for such refinement. The addition of the Schottky barrier was tested, because the tight binding scheme is, on its own, unable to describe additional electric potential coming from the redistribution of charge around the interface. We speculated that addition of the Schottky barrier could somewhat compensate for this fact and took the experimentally observed Schottky barrier as a good first guess to the electric potential due to the presence of the interface.

The Schottky barrier we added in some cases had a trapezoidal shape, as described in the first chapter. Characteristics of this barrier were obtained from the article [27].

For each possible configuration of iron tight binding parameters, Schottky barrier, and iron spin-orbit we determined the ratio $|K_{ui}/K_c|$, as well as the sign and magnitude of K_{ui} for one monolayer of iron grown on gallium-terminated GaAs. Values of these constants were obtained from TOTE calculations by a procedure described earlier.

Experiments show [22] that thin iron films on GaAs(001) exhibit a strong uniaxial anisotropy with easy axis along [110] direction. In our notation, this corresponds to $|K_{ui}/K_c| > 1$ and negative K_{ui}. If we assume that the relation (4.5) holds in the ultrathin region, then by extrapolating data from [22], which states values of anisotropy constants for d in the range 5–20 ML, we expect magnitude of K_{ui} around $3 \cdot 10^{-5}$ eV per iron atom.

We performed calculations with the energy integration step $\Delta\varepsilon = 0.004$ eV and 120×120 points in a Brillouin zone.[5] Results are listed in Table 4 — first three columns give the parametrization, whether we use spin-orbit coupling in iron and whether we include Schottky barrier; the latter three columns depict how our criteria were met in each case.

Parameters	Fe SO?	Schottky?	$\lvert K_{ui}/K_c\rvert$	$K_{ui} < 0$	$\frac{\lvert K_{ui}\rvert}{\mathrm{eV/atom}}$
Papaconstant. [10]	✓	×	$4 \cdot 10^{-3}$	×	$1 \cdot 10^{-1}$
	×	✓	$9 \cdot 10^{-5}$	✓	$2 \cdot 10^{-7}$
	✓	✓	$5 \cdot 10^{-2}$	✓	$5 \cdot 10^{-3}$
	×	×	$4 \cdot 10^{-4}$	×	$5 \cdot 10^{-5}$
Ext. Harrison [9]	✓	×	0.65	×	$2 \cdot 10^{-2}$
	×	✓	37.0	✓	$5 \cdot 10^{-5}$
	✓	✓	0.27	✓	$6 \cdot 10^{-4}$
	×	×	116	✓	$4 \cdot 10^{-5}$

Table 4: Choosing parametrization, iron spin-orbit and Schottky barrier.

Although the parametrization by Papaconstantopoulos includes larger number of fitting parameters, it is unable to reproduce the strong uniaxial anisotropy of the structure. For these parameters we tried to alter the distribution of atoms near the boundary by modeling a partial intermixing of GaAs atoms into iron, we changed the distance between iron and GaAs layers on the interface, we switched the geometric mean by which we obtain hopping parameters for Ga-Fe bonds for arithmetic mean, we investigated As-terminated surfaces, we experimented with adding second neighbour Ga-Fe interaction, but none of these changes was sufficient to reproduce the uniaxial character of anisotropy of the interface. We also tried improving convergence by increasing nk; however, no substantial improvement was achieved. For all possibile configurations we tried it was found that the magnitude of the fourfold anisotropy constant is significantly larger than the magnitude of the uniaxial anisotropy constant. As expected, the relative strength of the cubic anisotropy further increases with adding more iron layers. Because the uniaxial character of anisotropy of iron layers on GaAs(001) surface is the most distinct property of the magnetic anisotropy of this system, we conclude that usage of the parametrization from the reference [10] is not appropriate for investigation of magnetic anisotropies of thin iron films.

When we turn our attention to the extended Harrison parameters, we see that the situation is somewhat different, at least in the case we do not add spin-orbit

[5] Further we denote the number of points into which we divide the edge of the Brillouin zone as nk. Variable nk in the source code of the program gives half this value, for compatibility with adopted integration routines.

coupling into iron. In both cases without iron spin-orbit — with and without the Schottky barrier — we obtain strong uniaxial anisotropy that energetically favours [110] direction and has magnitude near the expected value. Because adding spin-orbit into iron again does not lead to correct character of the anisotropy, we conclude that in further computations we should not use spin-orbit coupling in iron. The question of Schottky barrier usage could not be resolved on basis of this test, as it could not be by any other of our calculations.

4.3 Gallium-terminated surface

After ruling out several possible alternatives, we investigated dependence of anisotropy constants K_i on the number of iron layers. We used the same settings as in the previous section, with the exception that we narrowed our focus on the extended Harrison parameters without spin-orbit coupling in iron. We investigated cases with and without Schottky barrier, with the same $\Delta\varepsilon = 4$ meV and nk = 120 as in the previous case.

After performing these calculations, we checked convergence of the results by recalculating anisotropies for the case of a single monolayer of iron for nk = 160 and obtained very good agreement with the results obtained with nk = 120. We also tested convergence with respect to the parameter $\Delta\varepsilon$, because densities of states typically possess large derivatives. Linear interpolation of results performed in order to obtain the anisotropies on the Fermi level can then easily become a source of error. For that reason we repeated all calculations with $\Delta\varepsilon = 0.04$ meV. In this run we obtained values of anisotropy constants given in the Table 5; dependence of K_{ui} on thickness of iron layer is drawn in Graph 1. The conversion rate between units of anisotropy is $100\,\mathrm{kJ/m^3} = 7.4\,\mu\mathrm{eV}$ per iron atom.

	Without Schottky barr.			With Schottky barr.		
Thickness (ML)	K_{ui} ($\mathrm{kJ/m^3}$)	K_{up} ($\mathrm{kJ/m^3}$)	K_c ($\mathrm{kJ/m^3}$)	K_{ui} ($\mathrm{kJ/m^3}$)	K_{up} ($\mathrm{kJ/m^3}$)	K_c ($\mathrm{kJ/m^3}$)
1	-497	-581	4.29	-588	-641	16.3
2	-261	-251	1.206	-143	-158	-2.33
3	-35.8	-55.4	-1.641	5.86	-24.7	-5.32
4	3.67	-15.8	-15.4	10.23	-3.14	1.25
5	16.5	9.10	0.681	29.4	14.9	0.91
6	-19.8	-25.6	4.07	-33.9	-48.9	-3.68
7	-81.6	-88.6	6.21	60.1	51.4	7.9

Table 5: Anisotropy constants for Ga-terminated surface

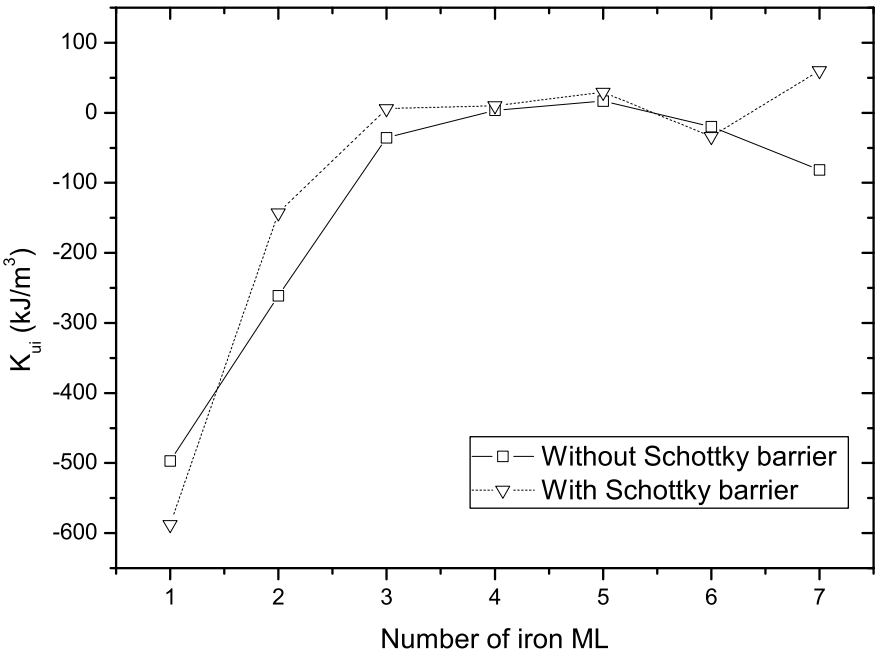

Graph 1: K_{ui} for Ga-terminated surface

When we compared these results with the results obtained for larger $\Delta\varepsilon$, we could see noticeable differences. These differences were typically far smaller than 2 kJ/m^3, but the differences for the 6 and 7 iron layers are two to five times larger. From it can infer that the choice of the energy mesh indeed plays an important role and must be handled with care. Therefore in all calculations we performed two runs of the program: In the first run we took large $\Delta\varepsilon$ and located the position of the Fermi energy. Then we performed the second run in the immediate vicinity of the Fermi level. This second run has small $\Delta\varepsilon$ and its results can be safely interpolated.

From the Graph 1 we see that for the first five ML the dependence of K_{ui} roughly corresponds to the expected behaviour predicted from the relation (4.5) — gradual convergence to zero. Nevertheless, for six monolayers we see a distinct dip, which departs from the expected behaviour significantly. We think that this deviation has its origin in using a relatively small number of GaAs atoms to represent bulk GaAs. In this respect we checked convergence for three iron ML; tests for larger system sizes (more than 6 Mn monolayers) are beyond this work and will be completed and presented elsewhere. Here we investigate only iron films

with thicknesses up to five monolayers, for which we tested that the results are well converged with respect to the number of GaAs layers used in our model (1–3 ML) or for which we inferred reasonably good convergence (4–5 ML).

To obtain quantitative data for the uniaxial anisotropy constant K_{ui}, we fitted dependence (4.5) to the results obtained for first five layers. If we compare the obtained results with the appropriate fit of the relation (4.5) (Graphs 2, 3), we see that this relation does not describe the calculated dependences faithfully. It is caused by the fact that K_{ui} changes sign at 3 or 4 ML thickness for system with or without Schottky barrier, respectively. It corresponds to an exchange of the easy axis of the system from [110] direction to $[1\bar{1}0]$, which is incopatible with the relation (4.5). For the thicknesses nearest to the turnover the uniaxial anisotropy is so small that our model even predicts fourfold anisotropy, instead of the expected twofold.

Fitted values of surface anisotropy constants are for the case with the Schottky barrier turned on

$$K^s_{ui,\mathrm{with}} = (-6.26 \pm 1.64) \cdot 10^{-5}\,\mathrm{J/m^2} \tag{4.7}$$

and

$$K^s_{ui,\mathrm{without}} = (-6.12 \pm 1.18) \cdot 10^{-5}\,\mathrm{J/m^2} \tag{4.8}$$

for the Schottky barrier turned off. The errors to the fitted constants are errors of the fit. These values are only slightly smaller than the experimentally observed value

$$K^s_{ui,\mathrm{exp}} = (-8.9 \pm 0.4) \cdot 10^{-5}\,\mathrm{J/m^3}\,, \tag{4.9}$$

but because of the poor match of the formula (4.5) with our data, this agreement should be only considered on a qualitative level.

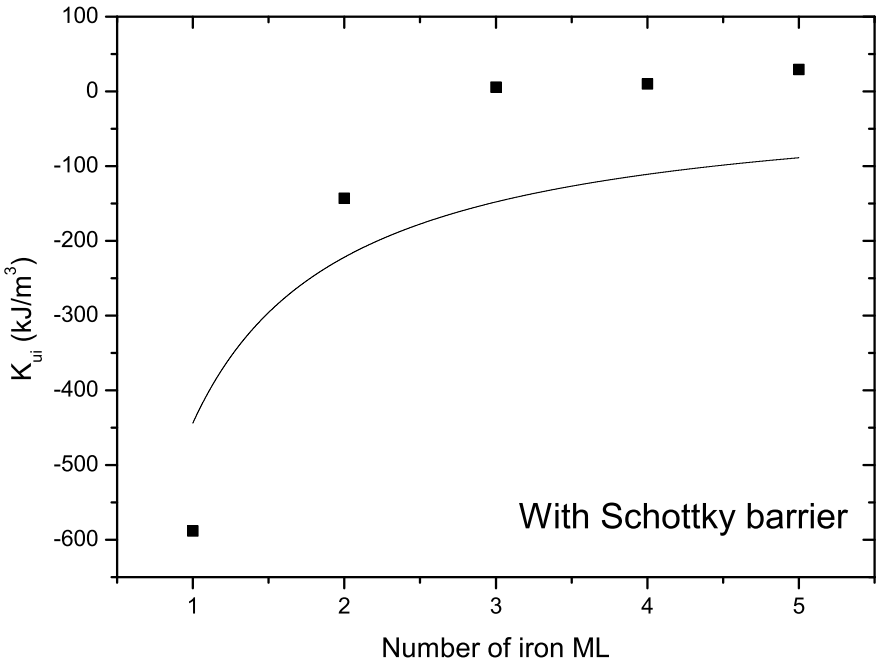

Graph 2: Uniaxial anisotropy for Ga-terminated surface, with Schottky barrier

To settle down how much the uniaxial anisotropy constant depends on the distance between last layer of GaAs and the first layer of iron, we repeated calculations with the Schottky barrier turned on for the distance 1.4449 Å between these two layers, instead of distance 1.4237 Å we considered in all other computations. Comparison of the results obtained with this new separation with the previous results is shown in Graph 4. We see that the results are almost identical; therefore, we can conclude that the output of our calculations is insensitive to the distance between iron and GaAs layers on the interface, at least to the changes of an order of 1.5 %. This was later confirmed also for As-terminated samples.

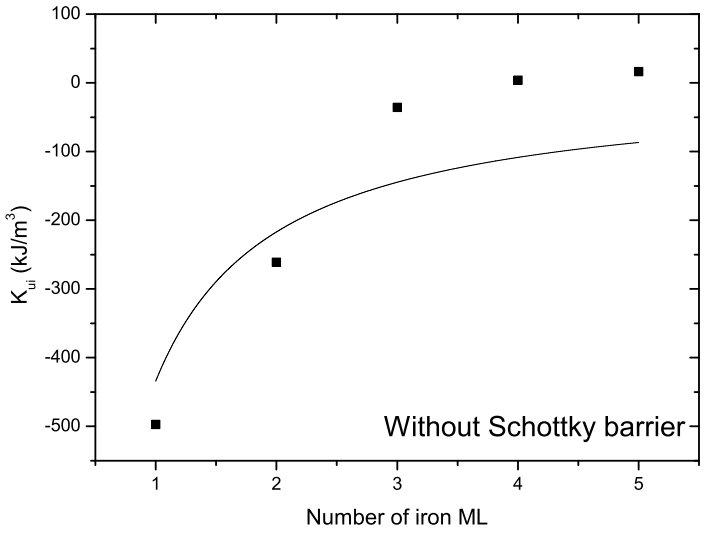

Graph 3: Uniaxial anisotropy for Ga-terminated surface, without Schottky barrier

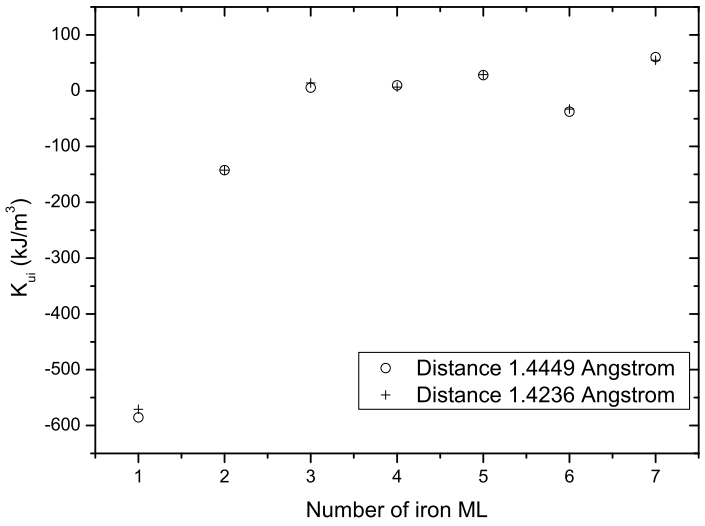

Graph 4: Dependence of K_{ui} on distance between GaAs and Fe layers on the interface

We further dealt with the problem of magnetic moment in iron layers to justify our estimate of shape anisotropy using the bulk Fe saturated magnetization. We investigated situation without the Schottky barrier for coverage up to 5 monolayers. Average magnetization in iron we obtained is visualized in Graph 5, distribution of magnetization among layers for iron film five monolayers thick is depicted in Graph 6. Values are given in Bohr magnetons (μ_B) per atom.

We see that the magnetization is relatively close to the bulk value 2.22 μ_B per atom [9], except for the case of one monolayer. For one ML coverage the shape anisotropy is about halved in comparison with the other coverages; however, shape anisotropy in this case is still sufficiently larger than any magnetocrystalline anisotropy obtained in our calculations. As a result, magnetization is forced to be in-plane in all investigated situations.

In the Graph 6 we can mention the typical behaviour of magnetization we observed — apart from the two layers nearest to the surface, there is almost no magnetic moment on gallium and arsenic atoms and even the two layers at the interface have magnetization small in comparison with iron layers. We can also notice that the magnetization of the iron layer nearest to the interface is diminished with respect to the other layers, which have magnetic moment enhanced in comparison with the bulk value.

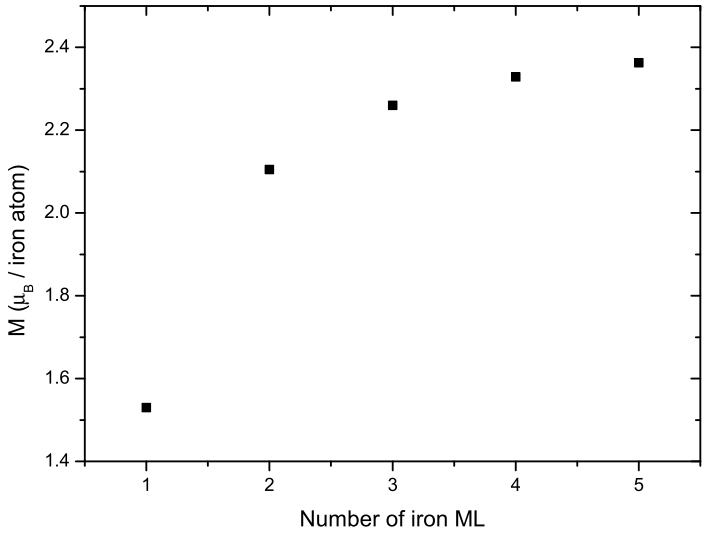

Graph 5: Average magnetization in iron layers

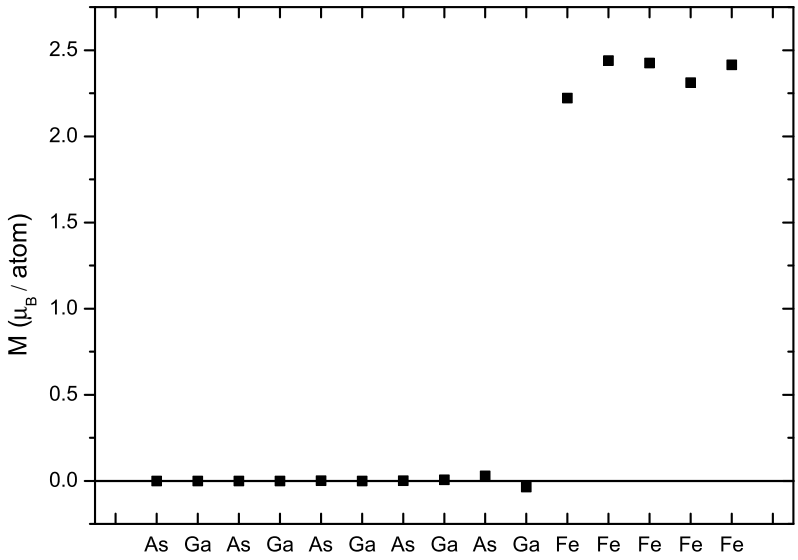

Graph 6: Dependence of magnetization on layer

4.4 Arsenic-terminated surface

After investigations of properties of interfaces terminated with gallium atoms, we turned our focus to the As-terminated interfaces. As was explained above, we investigated only the region 1-5 ML. We performed the calculations with the same settings we used for the Ga-terminated surface, with the single exception of interchanging the positions of Ga and As atoms.

From the total energies calculated by our program we extracted the values of anisotropy constants, their values are given in Table 6. Dependence of uniaxial anisotropy constant K_{ui} on the thickness of iron film is depicted in Graphs 7 and 8, together with our fit of the relation (4.5) to the calculated data.

Thickness (ML)	Without Schottky barr. K_{ui} (kJ/m^3)	K_{up} (kJ/m^3)	K_c (kJ/m^3)	With Schottky barr. K_{ui} (kJ/m^3)	K_{up} (kJ/m^3)	K_c (kJ/m^3)
1	-3515	-173	-10	-3171	14	-10
2	-1007	-250	-5.34	-1541	-367	-1.16
3	-711	-109	0.16	-1247	-267	1.97
4	-1038	-138	11	-803	-231	17
5	-608	-115	0.90	-1087	-161	47

Table 6: Anisotropy constants for As-terminated surface

If we compare these results with the anisotropy constants obtained for gallium-terminated surface, we see that our calculations predict larger uniaxial anisotropy for As-terminated surfaces. In contrast to the Ga-terminated samples, strong uniaxial anisotropy was found for all coverages. There seems to be no pattern among the values of four-fold anisotropy constant K_c predicted by our model, neither for As- or Ga-terminated surfaces. Anisotropy constant K_{up} is again small in comparison with the contribution of the shape anisotropy; therefore, the magnetization is again confined to the horizontal plane. Because of the negative sign of K_{ui}, [110] is predicted to be the easy axis of the system for all coverages, in agreement with experiment.

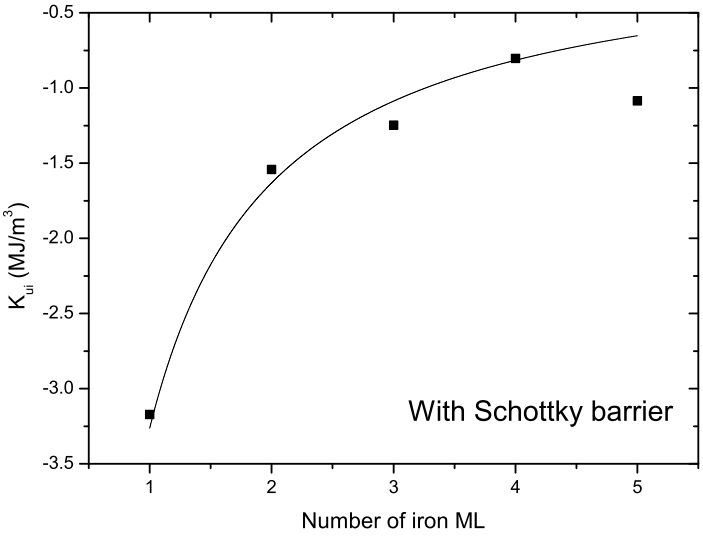

Graph 7: Uniaxial anisotropy for As-terminated surface, with Schottky barrier

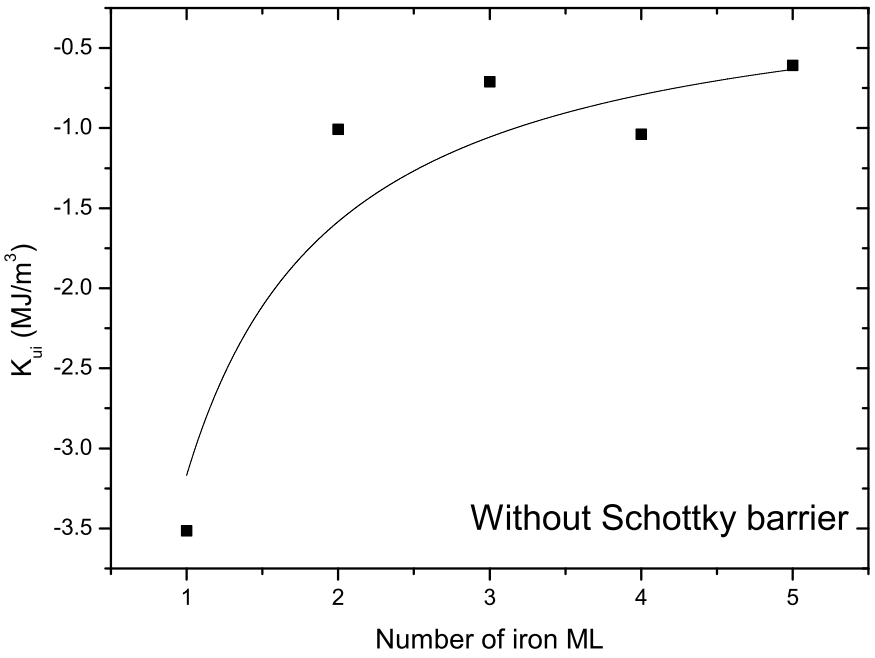

Graph 8: Uniaxial anisotropy for As-terminated surface, without Schottky barrier

In the case of As-terminated surfaces, formula (4.5) describes the uniaxial anisotropy constant relatively well. Corresponding values of K^s_{ui} — contributions of the interface to the uniaxial anisotropy — are

$$K^s_{ui,\text{with}} = (-46.0 \pm 2.6) \cdot 10^{-5}\,\text{J/m}^2 \tag{4.10}$$

in the case with Schottky barrier and

$$K^s_{ui,\text{without}} = (-45.6 \pm 4.2) \cdot 10^{-5}\,\text{J/m}^2 \tag{4.11}$$

without it. We can mention that these values are about five times larger than the experimentally measured values for Ga-terminated surfaces.

Chapter 5

Magnetic Anisotropies of Iron Layers on Ga(Mn)As

Adding a small admixture of manganese atoms into gallium arsenide leads to a splitting of the highest valence band near Gamma point of the Brillouin zone [28]. To account for this splitting Δ, we add exchange splitting (1.41) to the arsenic p-states (Jan Mašek, private communication). Because the states in the top of the valence band of pure GaAs are from approximately two thirds composed by the arsenic p-states [29],[1] we choose the exchange to be $\frac{3}{2}\Delta$, with the factor $\frac{3}{2}$ just canceling this coefficient of two thirds. For 5% admixture, the valence band splitting is equal to $\Delta = 152.3$ meV [30]. Because we altered our model in order to describe the vicinity of the Gamma point faithfully, eigenenergies calculated in points distant from the Gamma point can be inaccurate. However, more accurate microscopic description of manganese impurities in our model is problematic and beyond the scope of this work.

We repeated calculations of anisotropy constants for As-terminated surfaces of $Ga_{0.95}Mn_{0.05}As$ with and without incorporating Schottky barrier. Results obtained with and without manganese admixture can be compared in Graphs 9–10, which also present fits of dependence (4.5) to the results for impurity samples. Corresponding anisotropy constants K^s_{ui} are summarized in Table 7, together with the same data for pure GaAs substrate.

[1] In the sense of expansion of wavefunction in the basis of the atomic orbitals.

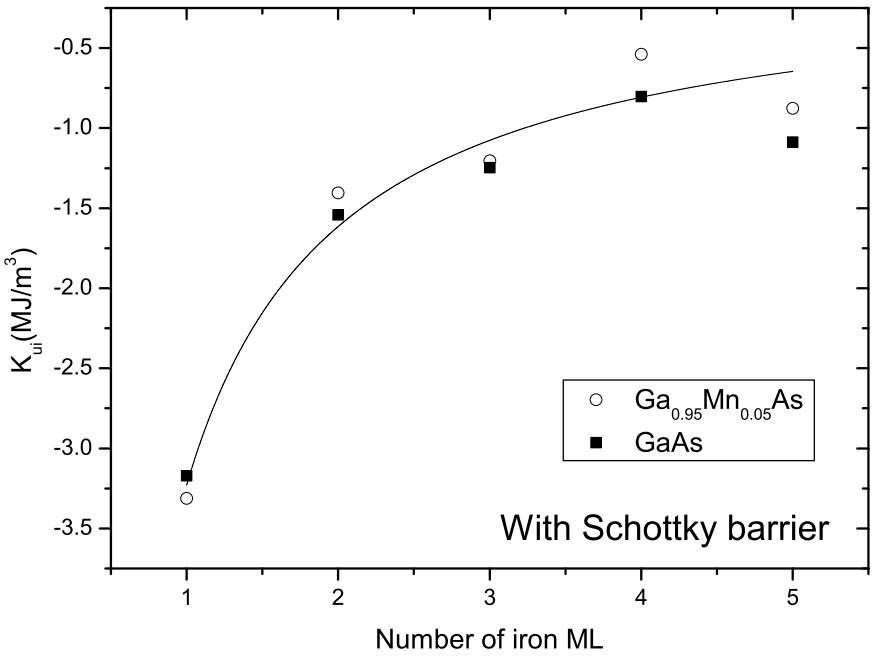

Graph 9: Effect of manganese impurity on uniaxial anisotropy, As-terminated surface with Schottky barrier

Manganese content	Schottky barrier	$K^s_{ui}\,(10^{-5}\mathrm{J/m^2})$
0 %	✓	-46.0 ± 2.6
	×	-45.6 ± 4.2
5 %	✓	-45.5 ± 2.6
	×	-45.6 ± 4.2

Table 7: Surface contribution to uniaxial anisotropy K^s_{ui} for $Ga_{1-x}Mn_xAs$ substrates

From the Table 7 we see that adding manganese impurities into GaAs does not change determined K^s_{ui} significantly. This is in agreement with recent experiments on all-epitaxial (Ga,Mn)As/Fe films [31]. However, comparison in Graph 10 indicates, that higher manganese admixtures could lower the anisotropies after turning on the Schottky barrier.

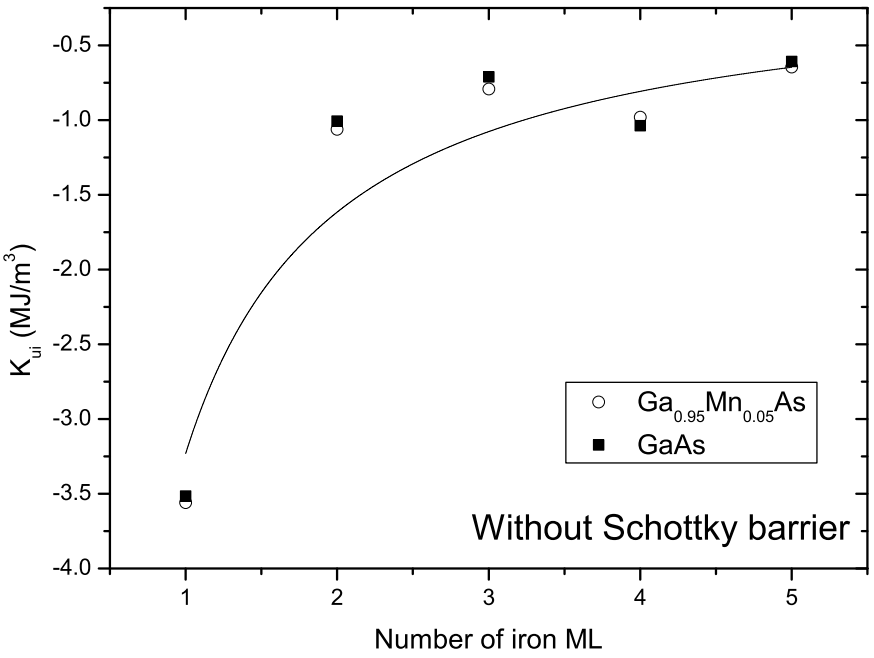

Graph 10: Effect of manganese impurity on uniaxial anisotropy, As-terminated surface without Schottky barrier

Chapter 6

Summary of Results, Discussion

We investigated magnetocrystalline anisotropy of thin iron films on GaAs and $Ga_{0.95}Mn_{0.05}As$ with the tight binding method. From the two tight binding parametrizations available we ruled one out, because it was unable to reproduce experimentally determined uniaxial anisotropy.

Uniaxial magnetic anisotropy constant K_{ui} of Ga-terminated samples approaches zero for large coverages, as expected according to the formula (4.5). However, we can observe deviations from the expected behaviour for higher coverages. We suppose that this discrepancy for 6–7 ML thickness stems from the small number of GaAs layers used in our simulations. We checked that we did not introduce significant error for 3 ML thickness; however, verifying convergence with respect to the number of GaAs layers for thicker films was beyond the scope of this work and will be reported elsewhere.

The anisotropy constant K_{ui} depends on the thickness of the iron film in agreement with the formula (4.5) for As-terminated surfaces, but this formula is unable to fully describe the dependence for Ga-terminated surfaces, due to easy axis direction reversal predicted by our model. This reversal is not seen in experiment which could be explained by deviations in real samples from the perfect interfaces assumed in our modeling. We, however, emphasize that the amplitudes of the uniaxial anisotropy are small when its sign starts to oscillate so the results of our modeling may not be significant in this range.

All anisotropy constants obtained with our program are several times smaller than the shape anisotropy of the thin film; therefore the magnetization is predicted to stay in the horizontal plane for all thicknesses and samples in agreement with experiment.

Uniaxial anisotropy was found to be significantly stronger in As- than in Ga-terminated GaAs surface. Since the vast majority of available experimental data is on Ga terminated samples, we were not able to compare this conclusion with

experiment.

Values of anisotropies obtained with Schottky barrier turned on and off are not dramatically different but, nevertheless, are appreciable. This points to a future study in which the calculated trends in the anisotropy as a function of the Schottky barrier height might provide useful information on the dependence of the anisotropy on doping in GaAs and/or on applied external electric fields. This result also indicates that redistribution of charge should be self-consistently taken into account in future studies of magnetic anisotropies in hybrid semiconductor-metal structures.

Finally, we investigated how adding Mn impurities into GaAs affects the anisotropies of As-terminated interfaces. No substantial change of values of K_{ui}^{s} was observed for GaAs substrate with 5% admixture of manganese, the easy-axis we obtained is again along the [110] direction in agreement with recent experimental studies of this ferromagnetic semiconductor – ferromagnetic metal structure. Our results indicate that the manganese impurities could, at larger concentrations, diminish the uniaxal anisotropy when the Schottky barrier is taken into account. However, with increasing concentration of Mn dopands the concentration of carriers in (Ga,Mn)As also increases which reduces the height of the Schottky barrier. A future systematic study of all these competing effects is therefore highly desirable in (Ga,Mn)As/Fe structures.

References

[1] K. P. McKenna: *The Simulation of the Electronic Transport Properties of nanoscale devices*, Ph. D. diss., University of Leeds, 2005.

[2] C. M. Goringe et al., Rep. Prog. Phys. **60** (1997), 1447–1512.

[3] M. J. Mehl, D. A. Papaconstantopoulos, in *Topics in Computational Materials Science*, edited by C. Y. Fong. World Scientific, Singapore, 1998.

[4] P. O. Löwdin, J. Chem. Phys. **18** (1950), 365–375.

[5] J. C. Slater and G. F. Koster, Phys. Rev. **94** (1954), 1498–1524.

[6] J. Formánek: *Úvod do kvantové teorie*. Academia, Praha, 2004.

[7] W.A. Harrison: *Electronic structure and the properties of solids*. Dover Publ., New York, 1989.

[8] J.-M. Jancu et al., Phys. Rev. B **57** (1998), 6493-6507.

[9] L. Shi, D. A. Papaconstantopoulos, Phys. Rev. B **70** (2004), 205101.

[10] D. A. Papaconstantopoulos: *Handbook of Electronic Structure of Elemental Solids*. Plenum, New York, 1986.

[11] J. Formánek: *Úvod do relativistické kvantové mechaniky a kvantové teorie pole /1*. Karolinum, Praha, 2000.

[12] K. H. J. Buschow, F. R. de Boer: *Physics of Magnetism and Magnetic Materials*. Kluwer Academic Publishers, New York, 2003.

[13] R. T. Tung, Materials Science and Engineering **R 35** (2001), 1–138.

[14] S. I. Kurganskii et al., Physica Status Solidi **129**, 293–299.

[15] J. Mol: Unpublished results.

[16] WWW: `http://www.netlib.org/lapack/`.

[17] T. Jungwirth: Unpublished results.

[18] G. Gilat, N. R. Bharatiya, Phys. Rev. B **12** (1975), 3479–3481.

[19] G. W. Tyler, Canad. J. Math. **5** (1953), 393–412.

[20] M. Singh et al., Phys. Rev. B **11** (1975), 287–294.

[21] G. Wastlbauer and J. Bland, Advances In Physics **54** (2005), 137–219.

[22] Kh. Zakeri et al., Journal of Magnetism and Magnetic Materials **299** (2006), L1–L10.

[23] M. Košuth et al., Europhys. Lett. **72** (2005), 816–822.

[24] M.T. Johnson et al., Rep. Prog. Phys. **59** (1996), 1409–1458.

[25] H. Ehrenreich: *Solid state physics*. Academic Press, London, 2001.

[26] Y. Ohta et al, J. Phys.: Condens. Matter **1** (1989), 2637–2646.

[27] Hanbicki et al., Appl. Phys. Lett **82** (2003), 4092–4094.

[28] H. Ohno et al., Appl. Phys. Lett. **73** (1998), 363–365

[29] P. Bogusławski, I. Gorczyca, Semicond. Sci. Technol. **9** (1994), 2169–2177

[30] T. Jungwirth et al., Rev. Mod. Phys. **78** (2006), 809—864

[31] K. Olejník et al., Phys. Rev. B **81** (2010), 104402